Oklahoma Water Research Institute

Annual Technical Report

FY 2000

Introduction

The Environmental Institute at Oklahoma State University has as its mission to serve as a center for stimulation and promotion of interdisciplinary research, graduate education, and public education relating to understanding, protecting, utilizing, and sustaining the natural environment. The University Center for Water Research (UCWR) is an integral part of the Institute's research effort, and is responsible for developing and coordinating water research funded through two programs: Oklahoma Water Resources Research Institute (OWRRI) funded by the U.S. Department of the Interior through the U.S. Geological Survey, and the Water Research Center (WRC) funded by the State of Oklahoma. The primary objective of the UCWR is the promotion of research of water related issues that are not only of national and regional concern, but also address the needs of Oklahoma.

The federally supported Oklahoma Water Resources Research Institute is one of 54 Water Institutes funded under Section 104 of the Water Resources Research Act. In Fiscal Year 2000, the $68,178 base grant to the OWRRI was directed to support one research project and water research administration and development activities as well as the information transfer program.

The research project was a cooperative effort jointly supported by the OWRRI, Oklahoma State University, and the U.S. Geological Survey District Office in Oklahoma City, OK. The project was designed to investigate and characterize factors affecting the channel stability of the Canadian River adjacent to the Norman, Oklahoma landfill. The USGS provided access to the extensive data already collected at the site as well as assistance with obtaining cores for the project. This project has provided an excellent opportunity for the OWRRI and OSU faculty to increase and improve interactions with USGS officials and researchers. A synopsis of this project is included in this report. The U.S. Geological Survey began a multi-disciplinary investigation in 1995 at the Norman, Oklahoma landfill as part of the Toxic Substances Hydrology Program, in collaboration with scientists at the Oklahoma State University, University of Oklahoma, and the Environmental Protection Agency. The contamination of the shallow alluvial aquifer at the Norman Landfill provides an exellent opportunity to study the spatial variability of biogeochemical processes and the resulting effects on the fate of degradable contaminants in the leachate plume. The vast number of landfill sites and ubiquitous nature of alluvial deposits make the results of this study highly transferrable.

Additionally, the OWRRI continued to oversee one Regional Competitive Grant program award. This project, awarded in FY 1997 to the University of Oklahoma and Texas A&M University, investigates geochemical and microbiological influences on biodegradation of pollutants in the subsurface. A synopsis of this project is included in this report.

Research Program

Basic Information

Title:	Geochemical and Microbiological Influences on Terminal Electron Accepting Processes and its Relation to the Biodegradation of Pollutants in the Subsurface: A Study of an Aquifer Contaminated by Landfill Leachate
Project Number:	G-02
Start Date:	9/1/1997
End Date:	2/28/2001
Research Category:	Water Quality
Focus Category:	Groundwater, Hydrogeochemistry, Toxic Substances
Descriptors:	Aquifer Characteristics, Anaerobic Treatment, Bacteria, Biodegradation, Biogeochemistry, Geochemistry, Groundwater Quality, Isotopes, Landfill, Microbiology, Pollutants, Toxic Substances
Lead Institute:	Oklahoma Water Research Institute
Principal Investigators:	Joseph M. Suflita, Ethan L. Grossman, Luis A. Cifuentes

Publication

1. Cozzarelli, I. M., J. M. Suflita, G. A.Ulrich, S. H. Harris, M. A. Scholl, J. L. Schlottman, and S. Christenson, 2000. Geochemical and Microbiological Methods for Evaluating Anaerobic Processes in an Aquifer Contaminated by Landfill Leachate. Environ. Sci. Technol. 34:4025-4033.
2. Elias, D. A., L. R. Krumholz,, R. S. Tanner, and J. M.Suflita, 1999. Estimation of Methanogen Biomass by Quantitation of Coenzyme M. Appl. Environ. Microbiol. 65:5541-5545.
3. Cozzarelli, I. M., J. M.Suflita, G. A.Ulrich, S. H.Harris, M. A. Scholl, J. L.Schlottman, and J. B. Jaeschke, Subsurface Contamination From Point Sources, in U.S. Geological Survey Toxic Substances Hydrology Program-Proceedings of the Technical Meeting, Charleston, South Carolina, March 8-12, 1999. Water-Resources Investigations Report 99-4018C, Volume 3 of 3, P. 521-530.
4. Grossman E.L., L.A. Cifuentes, and I.M. Cozzarelli, 2000, Rates of anaerobic methane oxidation in a landfill-leachate plume. Geol. Soc. America Abstracts with Programs, v. 32, p. A127
5. Grossman E.L., L.A. Cifuentes, and I.M. Cozzarelli, 1999. Modes of microbial methane oxidation in a landfill-leachate plume: Evidence from carbon isotopes. Geol. Soc. America Abstracts with Programs, v. 31, p. A391-A392.
6. Harris, S. H., G. A. Ulrich, and J. M.Suflita, Subsurface Contamination From Point Sources in U. S. Geological Survey Toxic Substances Hydrology Program-Proceedings of the Technical Meeting, Charleston, South Carolina, March 8-12, 1999. Water-Resources Investigations Report 99-4018C, Volume 3 of 3, p. 541-548.

Problem and Research Objectives: An environmental necessity, municipal landfills are a threat to local water quality as well as a contributor to global warming. In 1997 there were about 2500 landfills operating in the U.S., down from nearly 8000 in 1988 (Glenn, 1998). While the number of operating landfills is decreasing, the number of closed landfills is increasing, posing an increased risk of leachate contamination into underlying aquifers. Several studies have characterized the anaerobic environments of landfill leachate plumes (e.g., Baedecker and Back, 1979; Lyngkilde and Christensen, 1992; Ludvigsen et al., 1998; Cozzarelli et al., 2000). These plumes typically exhibit a succession of redox conditions with methanogenesis dominating near the source, followed downgradient by sulfate reduction, iron reduction, nitrate reduction, and oxygen reduction. The distribution of these redox states has a profound effect on the degradation of dissolved organic compounds. As a result, the accurate prediction of pollutant destruction in these environments requires precise observation of a number of ecological parameters including the activity of the resident microorganisms.

The work performed by implementation of this proposal has been to determine the presence and distribution of microbial processes that are occurring in the aquifer downgradient from the Norman landfill and to assess the impact of these processes on the quality of the groundwater. This project has been addressed in a variety of ways that include on-site field measurements and observations as well as laboratory experimentation and analyses. The findings are certainly not restricted to the Norman landfill. Many of our results will be useful to other investigators who are working in related areas at other field sites.

Methodology: This project involves the measurement of dissolved hydrogen gas in the groundwater downgradient from the landfill. We are investigating the usefulness of hydrogen as an indicator of the dominant microbial processes that could be occurring at the site. Information concerning the three-dimensional distribution of microbial processes is required in order to accurately describe a subsurface ecosystem and predict the rate of biodegradation of pollutant chemicals. Moreover, microbial activity often changes with time. Dissolved hydrogen measurements made over time may be a useful indicator of the dynamics of microbial communities in soil. If hydrogen can be used to make this description, then the task of characterizing the environment is greatly simplified. Traditionally, this characterization involves obtaining sediment cores that are used in laboratory experiments that can incur a significant expense while often requiring long incubation times and tedious sampling. Groundwater sampling for hydrogen is much simpler and cost effective in that no sediment is required. Water can be pumped from wells that have been installed at the site of interest and can then be removed after hydrogen monitoring is complete, resulting in minimal disturbance to the environment.

A thorough understanding of an aquifer environment requires information concerning the rates of the various microbial processes that are occurring. Often these rates are estimated from laboratory-based measures and extrapolated to the field. While estimating rates from laboratory incubations can be an accurate method, we have applied a more direct means for measuring metabolic activity at the landfill site. We have employed the push-pull test procedure in an effort to quantitate the microbial consumption rates of several compounds of environmental significance. Briefly, a push-pull test involves the removal of groundwater, which is stored in a carboy while chemicals of interest, including a conservative tracer are added after which the solution is reinjected into the formation. As samples are removed over time, the concentration of tracer and analyte will decrease due to microbial consumption and/or dilution. The degree of tracer loss due to dilution is applied to the concentration curve of the analyte. In this way, the decrease in analyte concentration that is due to dilution can be estimated. Any time-dependent decrease of the chemical of interest over and above that which can be attributed to dilution is then recognized as being due to microbial consumption and a rate is estimated based upon that measure. Some of the push-pull tests conducted thus far have examined the rate of sulfate and hydrogen consumption. Sulfate was examined because it is an important electron acceptor at the landfill site and is common to other aquifers as well. Moreover, the degradation of many pollutant chemicals is linked to the use of sulfate reduction as a terminal electron accepting process. Hydrogen is a critical intermediate in organic matter degradation affecting the nature of end products formed as well as the rate of organic carbon oxidation. Thus, describing the capacity of a given environment to process hydrogen is a key component to understanding overall carbon and energy fluxes in the area. In addition, we have used push-pull tests to measure uranium reduction rates in the aquifer. Although this aquifer is not contaminated with uranium, we are using the landfill site as a surrogate from which we can make predictions regarding the capacity of other locations to reduce and thereby immobilize soluble uranium.

A feature of natural systems that often complicates the estimation of rate processes at any site is the non-uniform distribution of microbial activity. We have recently removed cores of sediment from several locations downgradient from the landfill and are currently studying the two-dimensional distribution of sulfate reducing activity in incubations of this material. The spatial distribution of sulfate reduction activity can be visualized based on a direct imaging procedure that we have developed. Radioactive sulfate is applied to the face of a core sample; the sulfate is reduced by the resident microflora yielding radioactive sulfide that precipitates on the soil particles. The unreacted sulfate is then washed away leaving only sulfide, which can be examined qualitatively, and quantitatively using a specialized autoradiography instrument. This procedure allows for direct viewing of the distribution of microbial activity in a minimally disturbed sample giving the researcher an accurate representation of how the processes occur in the field.

Once the distribution of sulfate reduction activity has been observed, we can investigate the factors that limit sulfate reduction rates. Consequently, in addition to describing the distribution of activity at the site, this work will enhance our understanding of the underlying factors responsible for driving sulfate reduction at the landfill and other locations.

Molecular techniques are valuable tools for the characterization of microbial populations in soil. The various methods however must prove to be consistent and critically examined to assure their reproducibility. To that end, we have employed two popular methods of nucleic acid extraction for the examination of DNA present in sediment samples at the Norman landfill. Two locations at the landfill, designated 35 and 40 have been thoroughly examined previously and were thus chosen for this study. The first extraction method involved several freeze-thaw-grind cycles followed by an alcohol extraction and precipitation. The second method consisted of beat-beating, using the Bio101 FastDNA Soil Extraction kit (Qbiogene, Inc.). The DNA present in the sediment was purified from other components by binding to silica particles and washing by centrifugation with a series of buffers. Examination of the results from these different procedures will better define any limitations and inconsistencies that may exist when nucleic acid analysis of soil is necessary.

Stable isotopes have been widely used as tracers for methane oxidation (Grossman, 2001). Microorganisms preferentially consume $^{12}CH_4$ resulting in an enrichment of $^{13}CH_4$ in residual methane. Numerous studies have used stable carbon isotopes as a tracer for *aerobic* methane oxidation in landfill soils, but none have investigated anaerobic methane oxidation at a landfill site. We have used carbon isotopic measurements to investigate *anaerobic* methane oxidation in leachate-contaminated groundwaters at the Norman Landfill. We combined these results with hydrogeologic information to estimate the rate of natural attenuation of methane as it travels within the leachate plume. Isotope analysis was conducted on several water samples along the MLS35 to MLS80 transect using permanent multi-level samplers installed in 1997. We sampled for carbon isotopic analyses of dissolved inorganic carbon and methane in June 1998, April 1999, July-August 1999, and December 1999. The waters collected in April, 1999 were subject to a comprehensive array of chemical analyses. Sampling and analytical methods are described in Cozzarelli et al. (2000).

Principle findings and significance: Hydrogen measurements indicate that various bacterial processes are dominant at different locations within the field site. In fact, significant differences in hydrogen values were measured at different depths within the same well (Figure 1). In addition, we have found that dissolved hydrogen values change over time. We have monitored hydrogen levels at 35 different locations, taking a measurement approximately every six weeks for almost one year. Results suggest that the dominant microbial process is not constant over time, but changes with seasonal patterns, possibly as a function of groundwater temperature. Our work has shown that the concentration of hydrogen in groundwater can indeed be a useful indicator. However, under some environmental conditions its usefulness is limited and needs to be considered in concert with other groundwater geochemical measurements. Future work in this area will further define the usefulness of dissolved hydrogen measurements and provide an additional tool for site characterization to workers in several disciplines including microbiology, geochemistry and various engineering sciences.

Direct rate measurements made in the laboratory suggest that sulfate reduction and methanogenesis are the most important microbial reactions in the aquifer. At one location, the hydrogen values measured in the field agree with the laboratory experiments in predicting sulfate reduction as a dominant process (Figure 2). In another area of the aquifer, the hydrogen values implicate iron reduction as the dominant process but laboratory rate measurements could not confirm this prediction. This

finding implies that caution is necessary in the interpretation of dissolved hydrogen data and that other methods should be employed, in addition to hydrogen measurements, in efforts to accurately map the distribution of microbially catalyzed redox reactions.

Sulfate reduction rates based on the push-pull test method were found to be approximately 5 ?M/day (Figure 3). This value is in good agreement with laboratory incubations prepared using material from the same location. Our sulfate reduction rate estimates are similar to those measured at other sites. This finding confirms the integrity of the laboratory-based analyses and provides yet another method to estimate sulfate reduction activity. The advantages of the push-pull test are similar to that of dissolved hydrogen in that soil and expensive laboratory incubations are not necessary.

The degradation rate of higher molecular weight molecules in aquifers impinges on the rate and extent of hydrogen removal from the system. Therefore, accurate measurements of hydrogen consumption rates in soil are required for the precise definition of fate processes in groundwater environments. We used the push-pull test method discussed above to measure the hydrogen consumption rate at a particularly well-studied location at the Norman landfill. Our calculations included kinetic estimates of the K_m as well as measures of the maximum rate (Figure 4). We compared our values with those determined from other sites and found similar kinetic properties existed at different locations, suggesting that the hydrogen consuming capacity at the Norman landfill may be representative of other field sites.

In addition to determining the dominant microbial processes that are occurring at a site, the factors that limit the activity of the resident microorganisms also need to be investigated in order to maximize their biodegradative capacity. Sulfate-reducing bacteria are widely distributed in many environments and have the capacity to degrade compounds that are metabolized slowly or not at all under other electron-accepting conditions. We have found that sulfate reduction is an important process at the landfill and our experimental evidence has identified several factors that limit the rate of sulfate reduction at various locations in the aquifer. One of these factors is the concentration of sulfate. In some cases, simply adding exogenous sulfate to incubations of aquifer slurries increased the rate of sulfate reduction. At a different location, sulfate was available in excess but a push-pull test indicated sulfate reduction was very slow. When sediment cores were incubated in the laboratory, the addition of readily degradable organic matter in the form of lactate, resulted in increased sulfate reduction activity (Figure 5). Often overlooked is the ability of material from dead cells to supply nutrients and energy for live cells in soil environments. When a heat-killed suspension of sulfate reducing bacteria stimulated sulfate reduction, however, the addition of a live culture of sulfate reducers had a much smaller effect. These results indicate that at this location, the organisms capable of catalyzing the reduction of sulfate are present, but their activity is limited by the quality of electron donor. This limitation can be relieved upon the introduction of labile organic matter that may be in the form of lactate or even neighboring, dead cells.

Clay is a noteworthy component of sediments in many areas and microbial activity is believed to be relatively low in zones containing highly consolidated soils of low pore volume. Several locations within the aquifer at the landfill site have clay layers that extend horizontally for tens of meters and can have a vertical thickness of several centimeters or more. Because of the common incidence of clay at the landfill site and other locations, we have investigated the effect of this material on sulfate reduction rates in aquifer slurries supplemented with native clay as well as commercially available clay minerals. Incubations containing clay from the aquifer showed a high level of inhibition relative to incubations devoid of clay. Some of the purchased clays also affected a decrease in sulfate reduction rates with the level of inhibition dependent on the type of clay used. A standard treatment in the study of clay minerals involves washing the material with water prior to incubation. Washed clay exhibited an inhibitory effect that was statistically lower than that seen when unwashed clay was used. Moreover, the addition of the wash supernatant was found to inhibit sulfate reduction in pure cultures of sulfate reducing bacteria. The clay minerals found to exert the greatest inhibition were kaolin, barasym (a synthetic clay), and bentonite (Figure 6). Chemical analysis of these clays reveals relatively high amounts of aluminum oxide, a mineral common to clays but existing in various amounts depending on the source. We have identified aluminum oxide as a component that could potentially inhibit sulfate reduction. Indeed, sulfate reduction rates were lower when pure aluminum oxide (alumina) was added to incubations of soil, further suggesting that at least part of the inhibitory effect of clay material is due to the aluminum oxide content (Figudre 6). Inhibition was relieved by addition of a number of salts to mixtures of landfill sediment and bentonite clay suggesting a possible charge-related mechanism for inhibition. To investigate this

possibility, we are currently examining clay samples by scanning electron microscopy (SEM) in an effort to delineate the various mineral forms that may play a role in the distribution of charged species in the different clays.

Two rounds of push-pull tests were performed at the Norman Landfill to assess the extent of uranium reduction/immobilization under *in situ* conditions. The tests were designed to assess the impact of electron donors and alternate terminal electron acceptors (nitrate and sulfate) on the reduction of uranium. Addition of the electron donors formate, acetate, and lactate, did not appear to have any impact on uranium immobilization relative to the unamended well, suggesting that sufficient electron donor was present in the native groundwater to drive complete reduction of the added uranium (1.5? M). Slight inhibition of uranium immobilization by sulfate was observed, while nitrate was able to cause a more extensive inhibition of uranium immobilization. In a second round of tests, uranium and nitrate were injected at two nitrate concentrations (Figure 7). These tests were performed in wells that had been treated with uranium in the previous round of experiments. As nitrate reduction proceeded, previously immobilized uranium was apparently remobilized (Figure 7). Recent laboratory experiments suggest that intermediates in denitrification can oxidize uranium and are likely responsible for the remobilization observed in this experiment. Other work in this area has taken advantage of the ability of sulfate reducing bacteria to immobilize cobalt via sulfide precipitation. In soil cores amended with cobalt and radioactive sulfate, the areas where sulfide production occurred were visualized and soil samples from discrete locations within the cores were then removed for cobalt analysis (Figure 8). The areas that had high levels of sulfate reduction activity also showed a greater extent of cobalt immobilization indicating that the activity of sulfate reducing bacteria can play a role in detoxification of soil contaminated with cobalt.

The two DNA extraction procedures we performed indeed revealed inconsistencies that will be of interest to individuals working in this area of research. Using 5g of landfill sediment, the freeze-thaw method produced DNA pellets from both sites even upon five successive extractions suggesting that a single treatment may be insufficient for collection of a representative nucleic acid sample. We were not able to amplify the 16S rDNA gene using the first extraction from site 40. However, DNA from the well-characterized bacterium *Pseudomonas putida* was successfully purified by this method suggesting that the DNA from the landfill sample was not of PCR quality due to PCR inhibitors that were likely present in the site 40 soil sample. In contrast, we were able to PCR-amplify and eliminate the inhibition in the site 35 sample after further purification of the DNA using the silica-binding of the Bio101 Extraction kit. These preliminary results outline some of the current limitations associated with extracting and amplifying DNA from environmental samples and future work will further clarify measures necessary for success in this burgeoning field of research.

In addition to sulfate reduction, methanogenesis plays an important role in organic matter degradation at the landfill site. A thorough understanding of the role of methanogenesis often requires quantitation of the organisms. One of the methods used for quantitation of methanogen biomass takes advantage of the fact that an enzymmatic cofactor, coenzyme M (CoM) is found almost exclusively in methanogens. We collected landfill sediments from a thoroughly studied location at the site to use in efforts to standardize and simplify an existing procedure for CoM quantitation. The sediments showed an active methanogen population with 1.1 x 105 cells/g sediment and a CoM content per cell of 0.18 fmol CoM/cell which was lower than the average value of 0.41 fmol CoM/cell from all sites tested. In contrast to the previous procedure, our modification allows for quantitation of methanogen biomass within hours of sample collection and can be done aerobically, greatly simplifying the method.

It is noteworthy that we have successfully developed a sediment-free microbial enrichment capable of degrading cyclohexane carboxylate and cyclohex-1-ene carboxylate. These molecules are likely intermediates in the microbial degradation of several aromatic compounds. Therefore, the demonstration and characterization of this activity in the laboratory is fundamental to the description of aromatic compound destruction in contaminated environments. Current work with these enrichments involves the isolation of pure cultures whose degradative ability is affiliated with the reduction of sulfate, a common electron acceptor at the landfill as well as other sites including marine ecosystems where contamination by aromatic-containing fuels is a current dilemma.

Despite the prevalence of biologically produced methane, few studies have investigated anaerobic methane oxidation in aquifers. The alluvial aquifer adjacent to the Norman landfill provides an excellent opportunity for the study of anaerobic methane oxidation in a landfill-leachate plume. The redox indicators within the plume mimic the succession of energy yields for the various microbial reactions.

Within the plume core near the landfill, methane is present at high concentrations (up to 1135 µM), nearing saturation values (Table 1). Methane concentrations decrease above and below the plume, as well as downgradient within the plume (Figure 9). We have used analyses of ^{13}C, a stable isotope of carbon to investigate the evidence for methane oxidation in the leachate plume.

Carbon isotopic compositions of DIC (?$^{13}C_{DIC}$) within the 4/99 transect vary from –8.8 to +10.3‰ (Table 2; Figure 10). High ?$^{13}C_{DIC}$ values are typical for plume waters and almost always indicate methanogenesis (Grossman, 2001). These waters are also high in DIC concentration and alkalinity. The lowest ?$^{13}C_{DIC}$ values (= –5‰) are found in shallow wells at the downgradient end of the transect (MLS-80) and are representative of pristine groundwaters. The ?$^{13}C_{DIC}$ strongly correlate with DIC content, following a linear trend that cannot be explained solely by conservative mixing (Figure 11). Conservative mixing of the two end-members would generate a curved trend on a ?$^{13}C_{DIC}$ vs. DIC plot because plume waters are rich in DIC compared with native waters (Figure 11), and dominate the DIC reservoir. Methane oxidation may explain why the data fall below the mixing curve. Near the landfill, the low ?^{13}C of the methane (about –54‰), along with the fractionation associated with methane oxidation (about –14‰), will add ^{13}C-depleted DIC (roughly –68‰) to the groundwater. However, the effect of methane oxidation on ?$^{13}C_{DIC}$ is minor because of the low solubility of methane and large concentration of DIC in plume waters. On the other hand, oxidation of other dissolved organic carbon compounds undoubtedly contributes ^{13}C-depleted DIC. Another factor that may contribute to the deviation from the mixing curve is dissolution and precipitation of carbonate minerals. Carbonate minerals occur in low concentration in the sediments (~1%; G. Breit, pers. comm.). Mixing with waters from the slough plume and a secondary plume at MLS35-7 adds additional complexity to ?$^{13}C_{DIC}$ - DIC relationships.

Carbon isotopic compositions of methane (?$^{13}C_{CH4}$) range from –67 to +28‰ and show a progressive enrichment downgradient in all four sampling surveys (Figure 9, Table 1). Furthermore, ?$^{13}C_{CH4}$ increases at the upper and lower plume margins. Near the landfill (MLS35), methane within the plume has ?^{13}C values ranging from –51 to –56‰. The ?$^{13}C_{CH4}$ values within the plume axis increase from about –54‰ to –30‰ (MLS80-7). Over the same interval, methane concentrations decrease from 700 ± 200 mM to 85 ± 5 mM.

Declining methane concentrations can be explained by methane oxidation and by dilution with methane-poor native waters. However, dilution alone would not affect ?^{13}C values. Thus, the increasing ?$^{13}C_{CH4}$ values can only be explained by methane oxidation. On a ?$^{13}C_{CH4}$ versus log CH_4 concentration diagram, the trend for methane oxidation will approximate a straight line. Figure 12 shows the data for the April 1999 transect. Note that the plume and plume margins define two linear trends. The data for slough plume samples, near-surface samples, and background samples do not define a distinct trend because of mixing and variability in the initial concentration and initial ?^{13}C.

To determine the isotopic fractionation associated with methane oxidation, concentration data must be corrected for mixing. Hydrogen isotopic analyses were used to estimate the fraction of native water and thus calculate the original methane concentration. These data are only available for the April 1999 transect. Table 1 shows the methane concentrations corrected for mixing. After this correction, the plume and plume-margin waters continue to define two parallel linear trends (Figure 13). The aberrant plume-margin datum (in parentheses) is one of two plume margin waters with ?D and ?^{18}O values that do not fall on either the meteoric water line or the plume-native water mixing trend. Thus, the estimate of mixing based on ?D is likely compromised. The slopes of the regression for plume and margin water data define fractionation factors of 0.9864 ± 0.0010 and 0.9870 ± 0.0017, respectively. These equate to CO_2-CH_4 enrichment factors of –13.6 ± 1.0‰ and –13.0 ± 1.7‰, respectively. These two values are statistically indistinguishable and are within the range of values observed for aerobic methane oxidation (e.g., Barker and Fritz, 1981). For later calculations we will use the enrichment factor for the plume, –13.6‰, which is better constrained by the data. To our knowledge this is the first determination of the carbon isotopic fractionation associated with anaerobic methane oxidation in an aquifer system.

The fraction of methane remaining can be calculated based only on the carbon isotopic composition of the methane. No assumptions beyond those used to define the fractionation factors are required to calculate the fraction of methane oxidized. Figure 14 shows the percent methane oxidized along the MLS35-80 transect. At least 84% of the methane is oxidized in the 14 years it takes the plume to travel along the 210-m transect.

The rate of methane oxidation along the plume can be calculated using a first-order rate equation

$$d(CH_4)/dt = -k\,(CH_4) \qquad (4)$$

where k = the first-order rate constant. The rate constant equals the $-\ln [(CH_4)/(CH_4)_{0}]/t = -(\ln f)/t$, where t = time. To calculate f (fraction of methane remaining) we used the $?^{13}C$ of the methane for three segments of the transect. We used the flow rate (15 $m \cdot y^{-1}$; Scholl et al., 1999) to calculate t (Figure 14). The rate constants for the reaction vary from 0.06 to 0.23 y^{-1}, which yield half-lives for methane of 3 to 12 y. The 0.23 y^{-1} value is almost identical to that obtained in anoxic culture experiments with Big Soda Lake water (0.20 y^{-1}; Iverson et al.,1987). Rates were calculated from the rate constant x concentration. They vary from 18 $\mu M \cdot y^{-1}$ in the far reaches of the transect (MLS80) to 230 $\mu M \cdot y^{-1}$ in the mid-section of the plume where methane content is high and electron acceptors (SO_4^{2-}?) become available through mixing.

The methane oxidation rates calculated for the Norman Landfill site are three orders of magnitude lower than aerobic methane oxidation rates in water-saturated landfill sediments (Whelan et al., 1990; Figure 15). In terms of natural attenuation, aerobic oxidation is a far more efficient sink for landfill methane, than anaerobic oxidation. However, oxygen is relatively insoluble and is rapidly consumed in contaminated aquifers compelling the use of alternative electron acceptors for the oxidation of reduced compounds such as methane. The anaerobic methane oxidation rates observed at Norman Landfill are of the same order of magnitude as those in two other freshwater systems (Figure 15). In a Cape Cod aquifer, natural gradient tracer tests with nitrate as an electron acceptor yielded anaerobic oxidation rates of 150 $\mu M \cdot y^{-1}$ (Smith et al. , 1991). Anaerobic methane oxidation rates in the sulfate reducing zone of Big Soda Lake, Nevada were found to be of 18 to 31 $\mu M \cdot y^{-1}$ (Iverson et al. , 1987). In contrast, anaerobic methane oxidation associated with sulfate reduction in marine sediments (Hansen et al., 1998) and sediments within a marine-groundwater mixing zone (Bussmann et al., 1999) progresses at rates that are more than one to two orders of magnitude greater (6200 - 72,000 $\mu M \cdot y^{-1}$) than those of the freshwater systems. The greater rates noted for marine environments may be sustained by the increased availability of sulfate.

These data suggest methane is naturally attenuated as the landfill-leachate plume travels from the landfill to the Canadian River. Methane oxidation occurs by a novel anaerobic process that has not been previously characterized in an aquifer system. It is likely that other contaminants, such as chlorinated hydrocarbons, are cometabolized with this methane. Methane is anaerobically oxidized at rates of 18 to 230 $\mu M \cdot y^{-1}$, yielding methane half-lives of 3 to 11 years along the 210-m plume. These results demonstrate that anaerobic methane oxidation is viable sink for methane in contaminated aquifers. The mechanism for anaerobic methane oxidation in sulfate-reducing zones is hotly debated. Numerous studies have suggested possible mechanisms for methane oxidation on the absence of oxygen (Hoehler et al., 1994; Zehnder and Brock, 1980;Valentine and Reeburgh 2001). Allthough our data suggests this activity occurs in the aquifer, detailed studies of Norman Landfill microorganisms are required to investigate the mechanism for anaerobic methane oxidation. Further research is also required to investigate the role of anaerobic methane oxidation in the natural attenuation of toxic compounds such as chlorinated hydrocarbons.

Table 1. Concentration and carbon isotopic composition of methane in Norman Landfill groundwaters, along with hydrogen isotopic composition of water.

	April, 99	June, 98	April, 99		July-August, 99		December, 99		Mean			Mean		
Sample	?D in H2O	CH4 ?13C	CH4	CH4 ?13C	CH4	CH4 ?13C	CH4	CH4 ?13C	CH4 ? or MD^		N	CH4 ?13C	? or MD	N
	(‰)	(‰)	(uM)	(‰)	(uM)	(‰)	(uM)	(‰)	(uM)	(uM)		(‰)	(‰)	
MLS 35-2	-27.8	-43.8	56	-52.7			123	-31.2	89	34	2	-42.6	10.8	3
MLS 35-3	-15.4	-52.5	571	-53.6	1113	-54.7	936	-50.6	873	276	3	-52.8	1.7	4
MLS 35-4	-14.0	-54.1		-55.2	1138	-53.9			1138		1	-54.0		2
MLS 35-5	-9.8	-54.9	827	-55.3	1250	-54.8	349	-50.7	809	451	3	-54.0	2.3	4
MLS 35-6	-16.7	-21.9	28	-15.8	25	-8.6	34	-6.2	29	5	3	-13.1	7.1	4
MLS 35-7	-16.4	-31.9	70	-42.0	117	-41.3	2	-17.6	63	58	3	-33.2	11.4	4
MLS36-1	-41.5		13	-54.1					13		1	-54.1		1
MLS36-2	-26.8		23	-30.8					23		1	-30.8		1
MLS36-3	-25.6		142	-30.4	77	-13.1	400	-28.9	206	171	3	-24.1	9.6	3
MLS36-4	-15.4		532	-56.2	1131	-53.8	646	-47.2	770	318	3	-52.4	4.6	3
MLS36-5	-17.0		137	-51.6	205	-52.2	228	-43.4	190	47	3	-49.1	4.9	3
MLS36-6	-18.3		13	-7.8	13	7.2	14	-2.6	13	1	3	-1.1	7.6	3
MLS36-7	-18.0		13	-12.9	9	22.6	13	11.7	12	2	3	7.1	18.2	3
MLS37-1	-30.6													
MLS37-2	-21.1		23	-31.2			6	-8.0	15	9	2	-19.6	11.6	2
MLS37-3	-15.9		101	-43.8	481	-52.9	238	-49.0	273	192	3	-48.6	4.5	3
MLS37-4	-15.4		57	-40.1	57	-31.1	266	-44.4	127	121	3	-38.5	6.8	3
MLS37-5	-12.3		567	-53.8	1166	-54.7	621	-52.0	785	331	3	-53.5	1.4	3
MLS 37-6	-11.0		478	-52.8	1097	-52.5	899	-52.0	825	316	3	-52.4	0.4	3
MLS 37-7	-17.6		26	-12.7	32	-1.5	33	-13.0	30	4	3	-9.1	6.5	3
MLS 38-1	-44.1													
MLS 38-2	-25.2		30	-51.7					30		1	-51.7		1
MLS 38-3	-18.0		70	-47.3	374	-54.7	250	-46.0	231	153	3	-49.3	4.7	3
MLS 38-4	-15.2		185	-54.1	480	-56.5	70	-34.5	245	211	3	-48.4	12.1	3
MLS 38-5	-7.7	-48.9	569	-50.1	1147	-50.3	1005	-44.8	907	301	3	-48.6	2.6	4
MLS 38-6	-4.6	-48.8	724	-49.8	1383	-49.7	1244	-49.1	1117	347	3	-49.3	0.5	4
MLS 38-7	-10.8		202	-40.2	502	-43.0	282	-43.0	329	155	3	-42.1	1.6	3
MLS 40-3					1218	-52.1			1218		1	-52.1		1
MLS 40-4					113	-27.7			113		1	-27.7		1
MLS 54-1	-20.7													
MLS 54-2	-18.5		333	-54.1					333		1	-54.1		1
MLS 54-3			66	-50.0			6	5.8	36	30	2	-22.1	27.9	2
MLS 54-4	-17.1		19	-20.4			25	-1.4	22	3	2	-10.9	9.5	2
MLS 54-5	-14.2		41	-19.6			40	-13.9	41	1	2	-16.7	2.9	2
MLS 54-6	-12.3		128	-33.6			96	-27.6	112	16	2	-30.6	3.0	2
MLS 54-7	-11.5		224	-39.5			241	-38.4	233	9	2	-38.9	0.6	2
MLS 55-1	-46.2													
MLS 55-2	-29.5		7	-64.5					7		1	-64.5		1
MLS 55-3	-21.0		4	-35.3			370	-63.7	187	183	2	-49.5	14.2	2
MLS 55-4	-24.1		12	-48.0			6	-35.9	9	3	2	-42.0	6.1	2
MLS 55-5	-29.0		15	-41.4			16	-2.6	16	1	2	-22.0	19.4	2
MLS 55-6	-16.7	-25.4	105	-25.1			76	-24.7	91	15	2	-25.1	0.4	3
MLS 55-7	-11.9	-39.8	181	-36.8			168	-35.8	175	7	2	-37.5	2.1	3
MLS 80-1	-21.0													
MLS 80-2														
MLS 80-3	-21.2		TS*	TS					3		1	-34.3		1
MLS 80-4	-27.7		TS	TS					5		1	-53.9		1
MLS 80-5	-29.5		TS	TS					6		1	-52.6		1
MLS 80-6	-24.9		13	8.8			7	28.3	10	3	2	18.6	9.8	2
MLS 80-7	-12.6		89	-27.8			140	-32.4	115	26	2	-30.1	2.3	2
MLS NDP2	-33.6		TS	TS					1					
MLS NPD-5	-30.7		TS	TS					0					
MLS NPD-6	-32.0		TS	TS					0					
WLMLF	-3.5		1031	-52.9					1031		1	-52.9		1

*TS = too small to analyze. Blanks represent intervals not sampled. Many shallow wells either were above the water table or did not contain significant methane.

Table 2. Concentration and stable isotopic composition of Norman Landfill dissolved inorganic carbon (DIC).

Sample	June 1998		December 1999	
	DIC (mM)	?^{13}C (‰)	DIC (mM)	?^{13}C (‰)
MLS 35-2	46.8	11.6	62.3	6.2
MLS 35-3	51.8	13.3	48.1	9.0
MLS 35-4	43.3	10.0		
MLS 35-5	51.2	10.0	45.8	7.9
MLS 35-6	>60	7.1	34.6	6.0
MLS 35-7	>60	8.3	39.1	6.2
MLS37-2			32.1	7.6
MLS37-3			50.7	7.8
MLS37-4			51.2	8.4
MLS37-5			52.4	9.6
MLS 37-6			47.5	8.9
MLS 37-7			44.3	7.4
MLS 38-2	15.1	-5.5		
MLS 38-3	>60		45.8	7.5
MLS 38-4	11.9	9.6	49.7	7.4
MLS 38-5	53.2	10.3	47.5	10.4
MLS 38-6	6.4	11.0	58.5	10.3
MLS 38-7	>60		50.2	8.9
MLS 54-3			37.6	-0.2
MLS 54-4			37.4	1.9
MLS 54-5			48.3	7.4
MLS 54-6			51.8	7.8
MLS 54-7			47.3	9.1
MLS 55-1	6.4	-11.6		
MLS 55-2	>60	-9.3		
MLS 55-3	>60	-0.4	23.2	-3.0
MLS 55-4	>60	-1.5	28.2	1.9
MLS 55-5	11.4	-10.3	15.8	-5.9
MLS 55-6	47.0	7.3	53.9	7.5
MLS 55-7	46.9	9.4	50.0	8.4
MLS 80-4			18.2	-4.6
MLS 80-5			12.6	-8.8
MLS 80-6			31.6	2.3
MLS 80-7			50.1	9.2

Figure1. Hydrogen values change over time and depth in well # 35

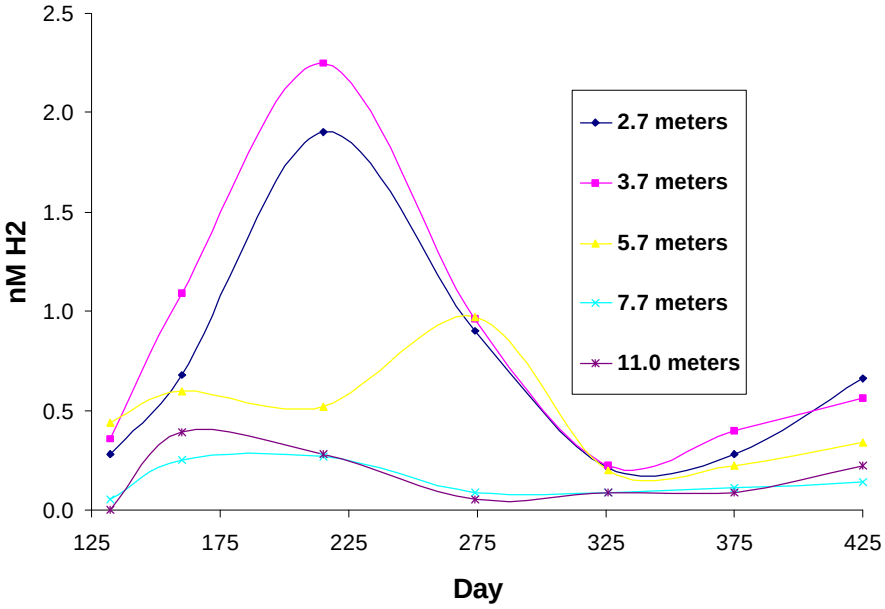

Figure2. Relationship between sulfate reduction and dissolved hydrogen in well # 35

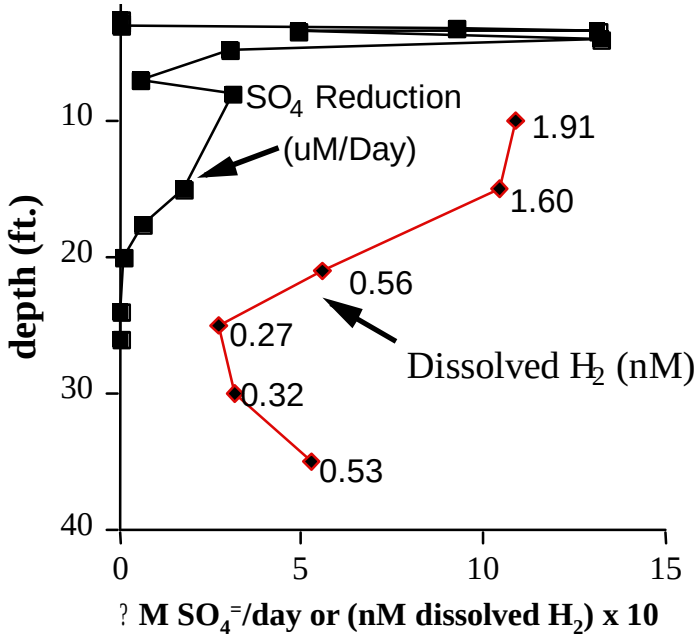

Figure 3. Sulfate consumption rate from push-pull test conducted near well #35.

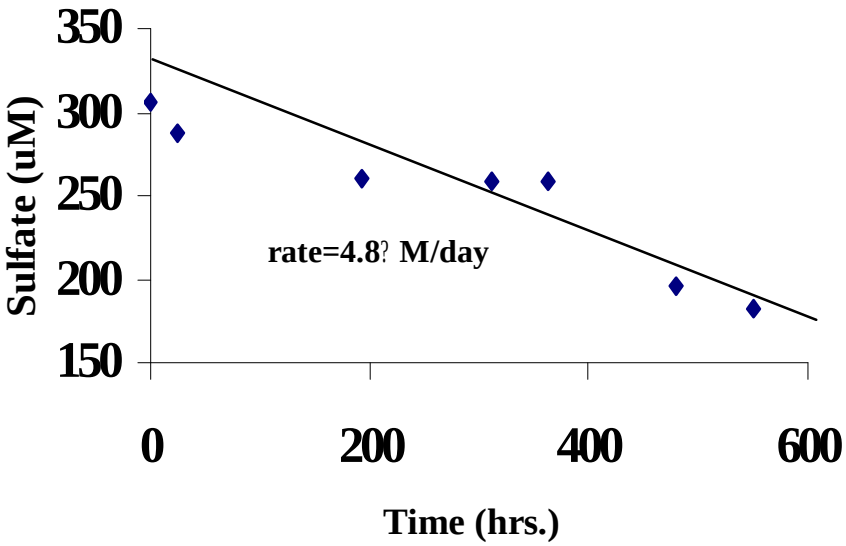

Figure 4. Hydrogen consumption curve from push-pull test conducted near well #35

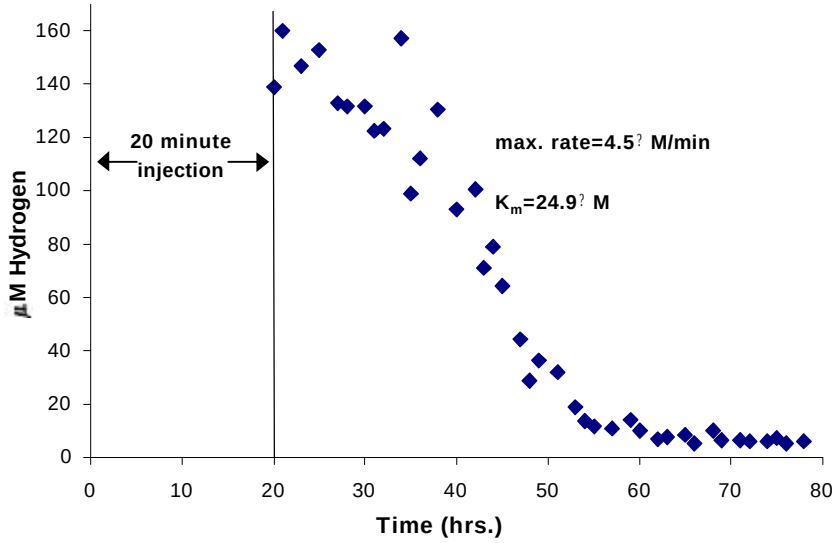

Figure 5. Sulfate reduction in an unamended core and in response to addition of electron donor and *Desulfovibrio* preparations.

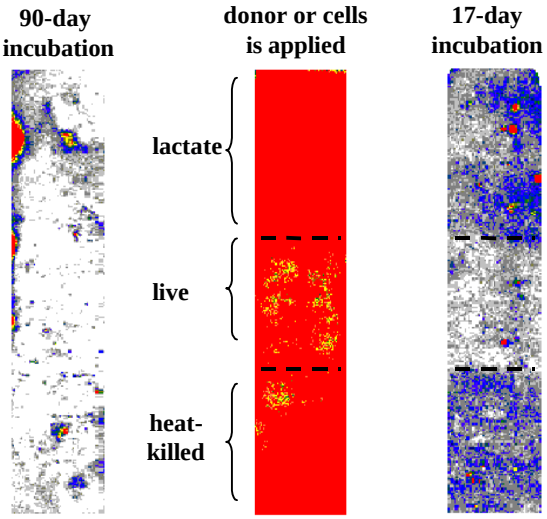

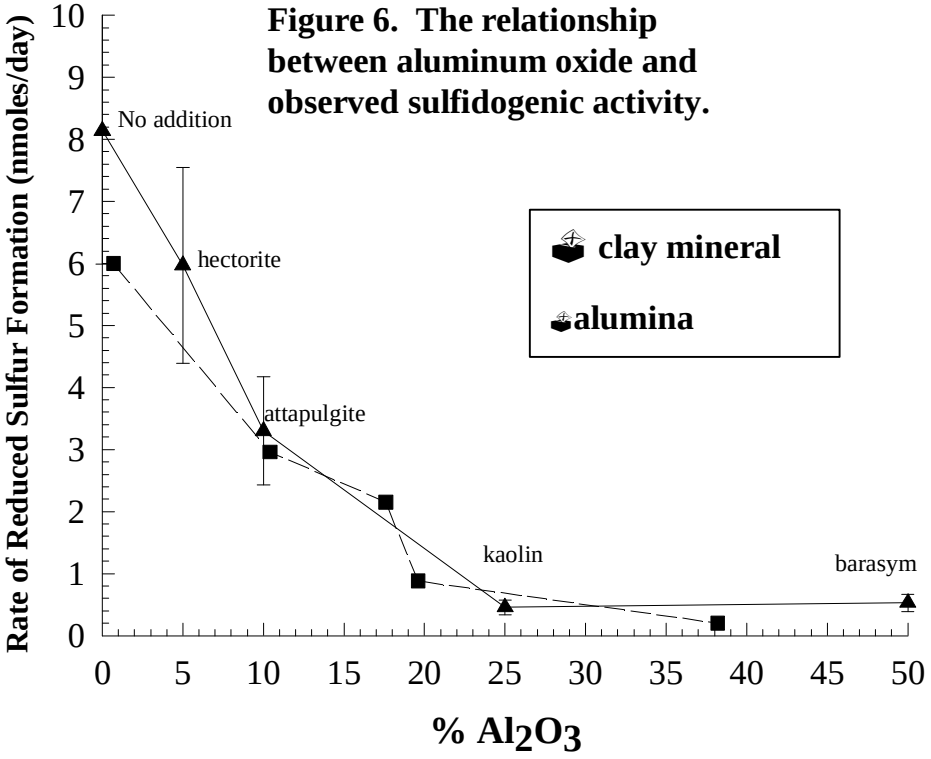

Figure 6. The relationship between aluminum oxide and observed sulfidogenic activity.

Figure 7. Effect of nitrate amendment on remobilization of uranium.

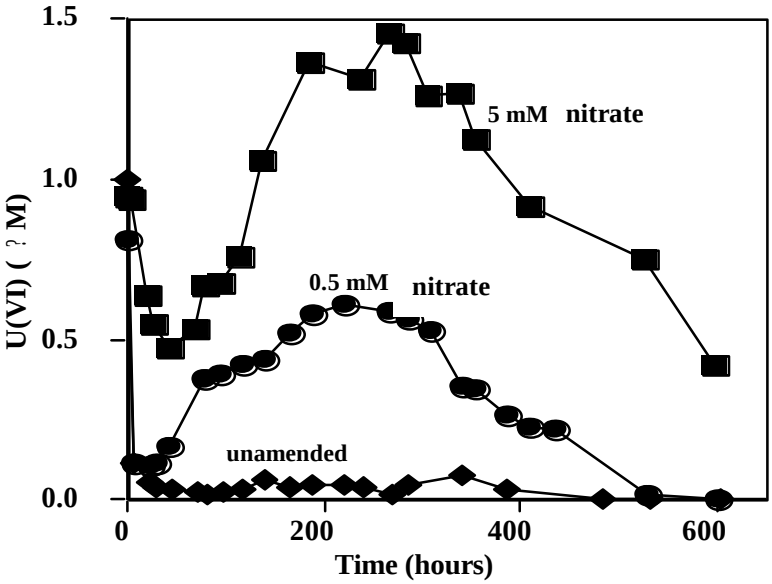

Figure 8. Sulfide production and corresponding degree of cobalt immobilization in cores from the landfill site

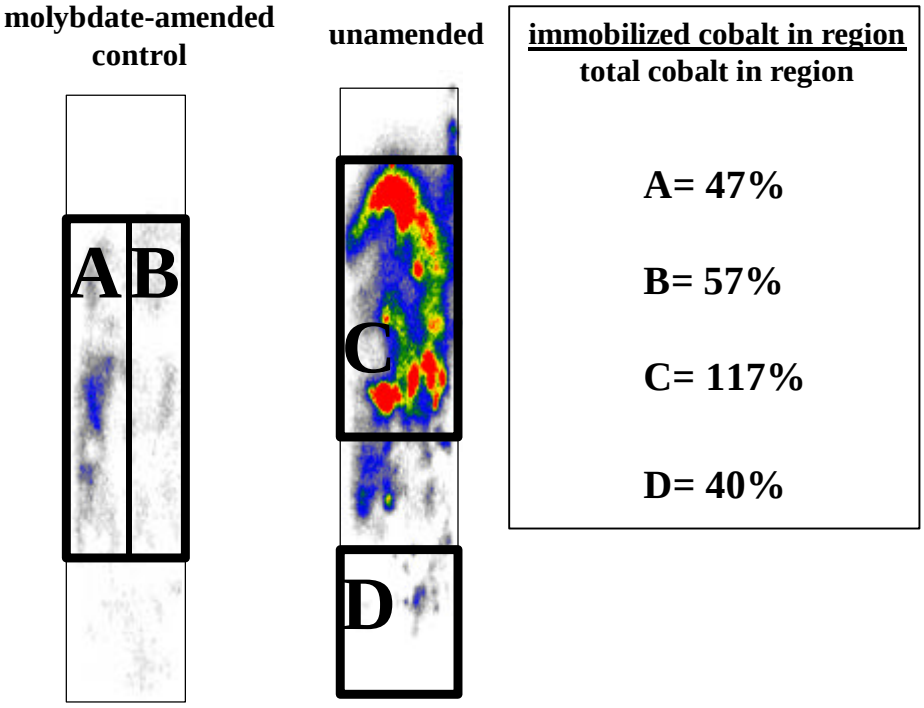

Figure 9. Distribution of methane and methane ? ^{13}C values across the MLS 35 to MLS 80 transect. Values are averages of all samples (Table 1).

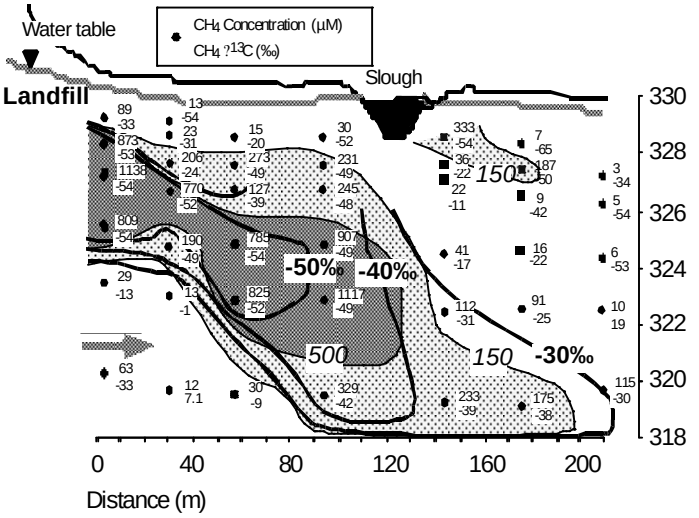

Figure 10. Distribution of dissolved inorganic carbon (DIC) and DIC? ^{13}C values across the MLS 35 to MLS 80 transect. Values are for the December 1999 transect (Table 2).

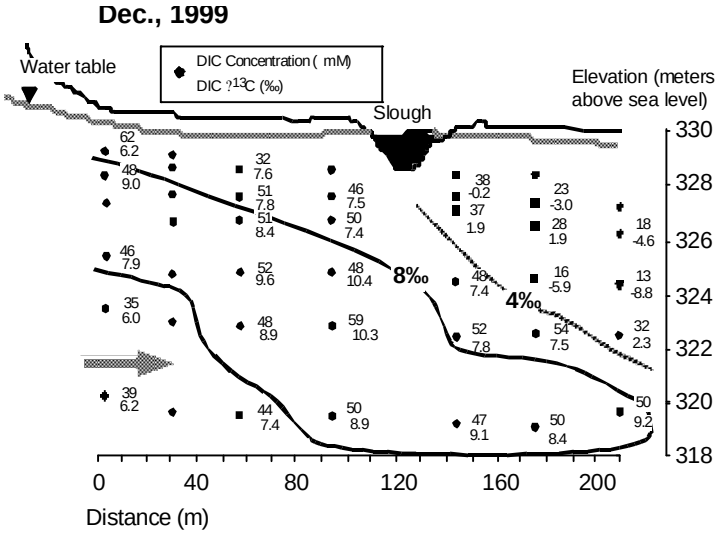

Figure 11. ? ^{13}C of DIC versus DIC content. Thick curve represents mixing between idealized landfill water (50mM DIC, 10‰ ? $^{13}C_{DIC}$) and native water (6.4mM DIC,-11.6 ‰ ? $^{13}C_{DIC}$). Arrow shows trend associated with methane oxidation in the vicinity of MLS 80-6.

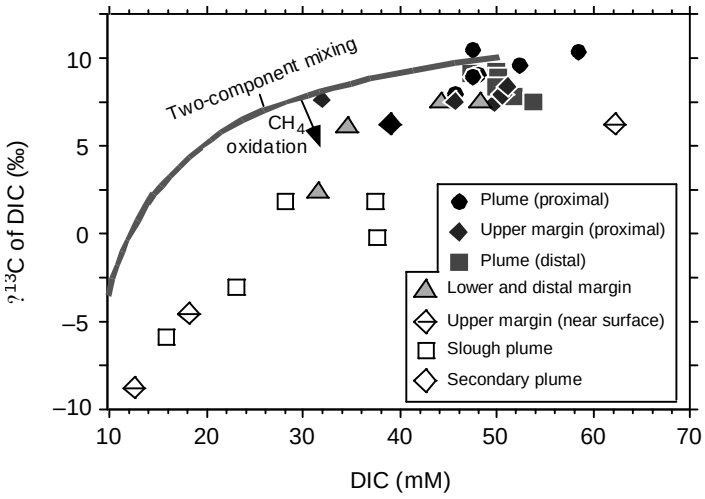

Figure 12. ? ^{13}C of dissolved methane versus methane concentration for April 1999 transect. Oxidation of methane in a closed system will yield a straight line on this plot. Symbols keyed to different parts of the transect.

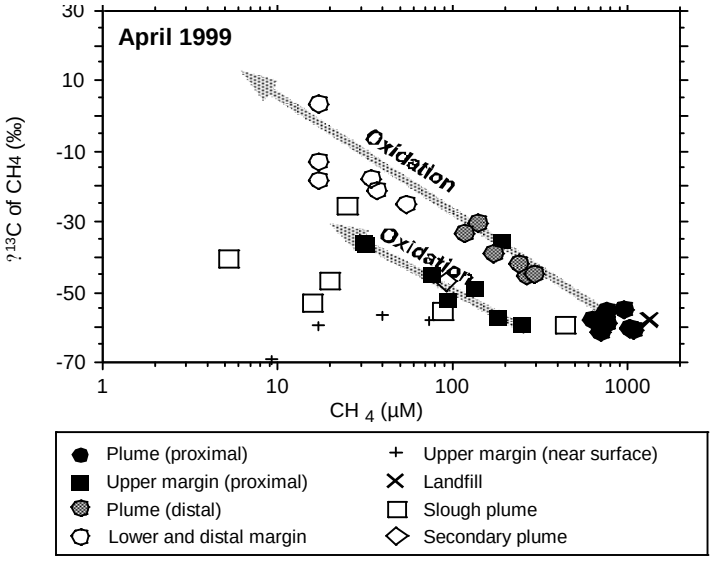

Figure 13. $\delta^{13}C$ **of dissolved methane versus methane concentration for April 1999 transect. Data are corrected for mixing using hydrogen isotopic composition of water as a conservative tracer.** CO_2**-**CH_4 **enrichment factor (s) for methane oxidation (with standard errors) calculated from regressions of plume and upper margin (proximal) data. Symbols defined in figure 5.**

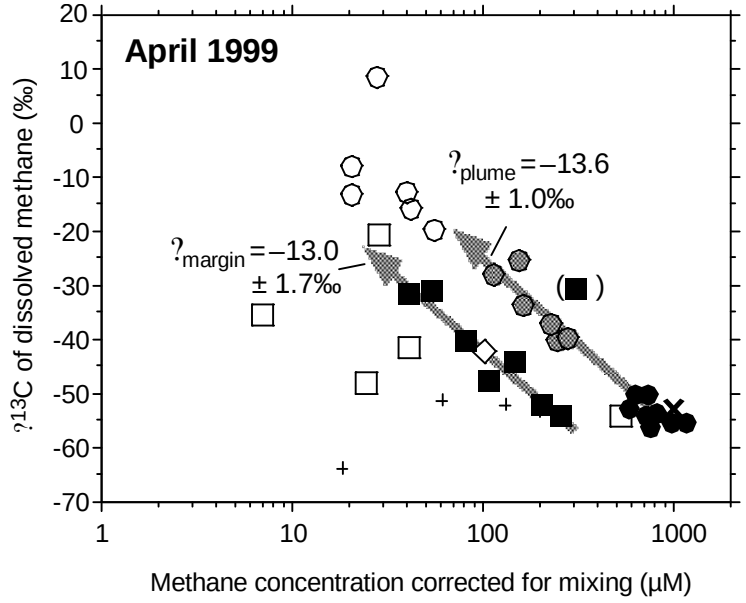

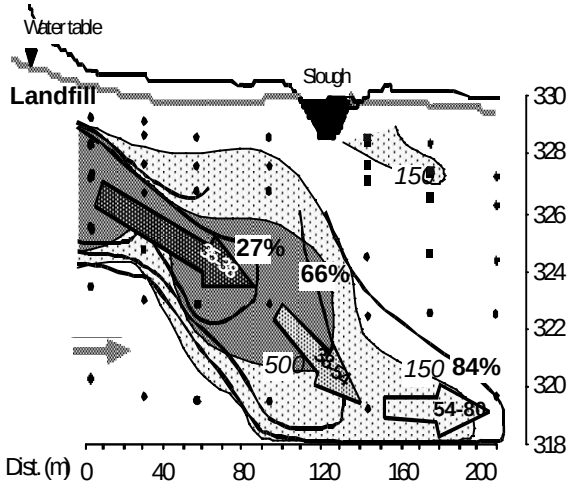

Wells	MLS35-38	MLS38-54	MLS54-80
k(1°) (y^{-1})	0.06	0.23	0.16
Half-life (y)	10.9	3.0	4.5
R(1°) (µM y^{-1})	~56	47 - 202	16 - 32

Figure 14. MLS 35-80 transect with countours for methane content (italics) and percent methane oxidized (bold; from $\delta^{13}C$ **contours). Also shown are the three segments modeled for anaerobic methane oxidation rates, and the rate constants, half-lives, and rates.**

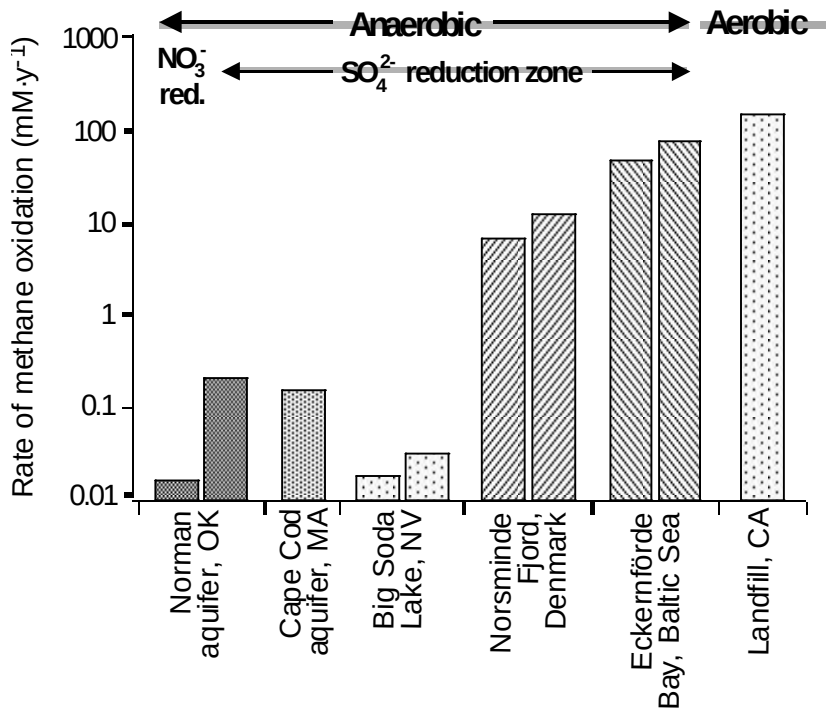

Figure 15. Comparison of rates of methane oxidation in the Norman aquifer leachate plume, Cape Cod aquifer (Smith et al., 1991), Big Soda Lake (Iverson et al., 1987), Norsminde Fjord (Hansen et al., 1998), Eckernförde Bay (Bussmennet et al., 1999). Where two bars are shown, data are minima and maxima.

REFERENCES

Baedecker, M. J.; Back, W. *Ground Water* **1979**, *17*, 429-437.

Barker, J. F.; Fritz, P. *Nature* **1981**. *293*, 289-291.

Bussmann, I.; Dando, P.R.; Niven, S. J.; Suess, E. *Marine Ecology Progress Series* **1999**, *178*, 169-177.

Cozzarelli, I. M.; Suflita, J. M.; Ulrich, G. A.; Harris, S. H.; Scholl, M. A.; Schlottmann, J. L.; Christenson, S. . *Environ. Sci. Technol*. **2000**, *34*, 4025-4033.

Glenn, J. *BioCycle*, **1998**, *April*, 32-43

Grossman, E. L., **2001**. Stable carbon isotopes as indicators of microbial activity in aquifers, in Manual of Environmental Microbioloby, 2nd ed., C. J. Hurst et al., (eds.), American Society for Microbiology Press, Washington, DC (in press).

Grossman, E. L. *Ph.D. Dissertation*, University of Southern Caalifornia **1982**.

Hackley, K.C.; Liu, C.L.; Coleman, D.D. *Ground Water* **1996**, *34*, 827-836.

Hansen, L. B.; Finster, K., Fossing, H.; Iverson, N. *Aquatic Microbial Ecology* **1998**, *14*, 195-204.

Iverson, N.; Oremland, R. S.; Klug, M. J. *Limnol. Oceanogr*. **1987**, *32*, 804-814.

Ludvigsen, L.; Albrechtsen, H.-J.; Heron, G.; Bjerg, P. L.; Christensen, T. H. *Jour. Contam. Hydrol*. **1998**, *33*, 271-291.

Lyngkilde, J; Christensen, T. H. *Jour. Contam. Hydrol*. **1992**, *10*, 273-289.

Scholl, M. A.; Cozzarelli, I. M.; Christianson, S. C.; Breit, G. N.; Schlottmann, J. L. *U.S. Geological Survey Toxic Substances Hydrology Program, Proceedings of the Technical Meeting, Charleston, SC, March 8-12, 1999–Vol. 3, Subsurface Contamination from Point Sources;* Morganwalp, D.W., and Buxton, H.T., Eds.; Water-Resources Investigations Report 99-4018C; U.S. Geological Survey: West Trenton, NJ, 1999; pp 557-568.

Schlottmann, J. L.; Scholl, M. A.; Cozzarelli, I. M. *U.S. Geological Survey Toxic Substances Hydrology Program, Proceedings of the Technical Meeting, Charleston, SC, March 8-12, 1999–Vol. 3, Subsurface Contamination from Point Sources;* Morganwalp, D.W., and Buxton, H.T., Eds.; Water-Resources Investigations Report 99-4018C; U.S. Geological Survey: West Trenton, NJ, 1999, pp 509-520.

Smith, R. L.; Howes, B. L.; Garabedian, S. P. *Appl. Environ. Microbiol*. **1991**, *57*, 1997-2004.

Whelen, S. C.; Reeburgh, W. S.; Sandbeck, K. A. *Appl. Environ. Microbiol*. **1990**, *56,* 3405-3411.

Valentine, D. L.; Reeburgh, W. S. *Environmental Microbiol*. **2000**, *2*, 477-484.

Zehnder, A. J. B.; Brock, T. D. *Jour. Bacteriol*. **1980**, *137*, 420-432.

Basic Information

Title:	Geomorphology and Sedimentology of the Canadian River Alluvium Adjacent to the Norman Landfill, Norman, Oklahoma
Project Number:	B-02
Start Date:	3/1/2000
End Date:	2/28/2001
Research Category:	Ground-water Flow and Transport
Focus Category:	Geomorphological Processes, Sediments, Toxic Substances
Descriptors:	geomorphology, sedimentology, permeability, landfill, toxic substances
Lead Institute:	Oklahoma Water Research Institute
Principal Investigators:	Richard A. Marston, Stanley T. Paxton

Publication

Problem and Research Objectives:

The Norman City Landfill is a closed municipal landfill located on the floodplain of the Canadian River in Norman, Oklahoma. The landfill accepted solid waste from the city between 1922 and 1985, at which time it was closed with a vegetated clay cap. The landfill was never lined, so at least one leachate plume has developed and now extends southward into the floodplain alluvium toward the Canadian River. The alluvium is 10 to 15 meters thick and composed of unconsolidated sediments ranging from clay to gravel. The water table is found at a depth of about 1 meter. The alluvial aquifer is underlain by the Hennessey Shale, which acts as a confining unit.

The geomorphic and sedimentologic characteristics of the floodplain and active channel have yet to be documented. These characteristics will control the permeability of the floodplain, and therefore, the migration potential of leachate plumes, known and unknown. Inspection of historical aerial photographs reveals that the Canadian River has experienced significant horizontal migration over the past few decades in the region of the Norman Landfill, initiating episodes of erosion and deposition. Lateral channel instability is expected for a sand-bed, meandering river, but bank protection has truncated meander migration. Understanding channel stability would enable more informed judgments about the likelihood that stream erosion could mobilize contaminants from the landfill in particulate form. We might anticipate a correspondence between spatial and temporal patterns of channel stability and the vertical and horizontal connectivity of alluvial units.

Objectives

The objectives of our proposed research were to describe and explain:

1) the vertical and horizontal heterogeneity in texture of floodplain alluvium to facilitate understanding of permeability pathways; and
2) the geomorphic stability of the Canadian River upstream, adjacent, and downstream of the Norman Landfill in a manner that can be used to assess past and future mobility of contaminants in particulate form.

Study Area

The Canadian River begins in the Sangre de Cristo Mountains of southeastern Colorado and flows 1460 km to its confluence with the Arkansas River in eastern Oklahoma. In the vicinity of the Norman Landfill, the Canadian River is a low-sinuosity, sand-bed river that alternates between braiding and meandering in pattern. In central Oklahoma, the Canadian River Valley ranges in width from 2.5 to 6.5 km, and is composed of two geomorphic surfaces: a late Holocene valley fill and the modern floodplain. The Norman City Landfill is situated on the north side of the Canadian River, south of the City of Norman, between Chautauqua and Jenkins avenues. The base of the landfill is 3.5 meters above the thalweg of the river. The valley fill is approximately 10-15 meters deep and composed of unconsolidated sediments ranging from clay to gravel. The aquifer is underlain by the Hennessey Shale, which acts as a confining unit.

Methodology:

Sedimentology

The first project objective, concerning sedimentologic controls on permeability pathways, was accomplished by completing five tasks:

1) collect cores and conductivity logs from the floodplain alluvium;
2) describe and photograph the cores;
3) perform textural analysis on each core based on lithofacies;
4) determine the relationship between texture and permeability using established equations; and
5) interpret the conductivity logs for texture based on the cores and creation of a 3-D model of permeability based on log interpretation and textural analysis.

Obtaining Conductivity Logs and Cores

A sampling grid was designed to obtain uniform coverage of the floodplain alluvium. The grid was composed of cross-lines, which ran parallel and perpendicular to the Canadian River. Geoprobe? conductivity logs were taken along these cross-lines to a depth of 10 to 12 meters (35 to 40 feet), and the average distance between the sample locations was about 37 meters (110 ft). A total of 78 conductivity logs were taken, and continuous cores were taken in 19 of these wells. A hand-held GPS system and map were used to locate each of the sampling locations. This GPS system could locate the latitude and longitude of each site to within 1 m (3 feet). After the samples were collected from each site, the site of each well on the floodplain was marked. A second GPS system was used by Scott Christenson from the USGS office in Oklahoma City to obtain more accurate readings. Christenson was able to measure the latitude (X), longitude (Y), and surface elevation (Z) of each well to within 2 cm. The set of readings taken by Christenson provided the X, Y, and Z data for each well in the project.

Conductivity Logs

Seventy-eight conductivity logs were collected using a Geoprobe®. A Geoprobe® is a hydraulically powered, percussion soil probing instrument. The Geoprobe® uses static weight and the percussion force of a soil probing hammer to advance a direct-push electrical-logging probe through the subsurface. The Geoprobe® is attached to a vehicle, which provides the static weight for the instrument. The direct-push e-logging probe is attached to the leading end of a tool string and advanced into the subsurface. The probe used is a Wenner array design that is 38 cm (15 inches) long with a maximum diameter of 3.8 cm (1.5 inches). The electrical conductivity data is transmitted to a field computer, which is attached to the Geoprobe® via a cable. The conductivity is measured in millisiemens/ft. Conductivity readings are taken every 1.5 cm (0.05 feet) and the computer displays a real-time log on its screen as the log is taken. In addition to conductivity, the system also records the rate of penetration. We discuss our data in both feet and meters because the Geoprobe measurements are taken in feet.

Once the conductivity log data was collected, it was imported to an Excel spreadsheet. In Excel, the log data was plotted as a curve with depth and printed out on oversize paper. The logs were pieced together to form the cross-sections of the study area. These cross-sections were then correlated based on the following criteria:

1) vertical position of sands relative to mud layers
2) vertical variations in texture based on sieve analysis
3) depositional subenvironments.

The macro-cores provided a check between the conductivity logs and the actual lithology. However, there was no age control available for the cores that were collected. Therefore the strata of the conductivity logs were matched based on similar lithologic characteristics observed in the cores. The sieve data was also used to match similar strata based on the premise that

similar lithologies will exhibit similar texture. Missing sections in the cores due to compaction and poor recovery provided problems for correlation. It was impossible to check the conductivity log data against known lithology for the sections that were missing.

Nineteen continuous cores were collected using the Geoprobe®. The Geoprobe® yielded cores of alluvium in 1.2-meter (4-foot) depth intervals. The total depth of each cored well ranged from 11 to 12.2 meters (6 to 40 feet) encompassing the entire thickness of the floodplain alluvium. The Geoprobe® uses a macro-core piston rod soil sampler. The macro-core sampling tube is 122 cm (48 inches) long and 5 cm (2 inches) in diameter. The sampling tube contains a removable polycarbonate core liner that is 3.8 cm (1.5 inch) in diameter. The sampling tube also contains a piston rod, which keeps the sampler sealed until the desired depth is reached for each sample interval. The piston rod sampler is designed to enhance the recovery of unconsolidated materials. However, complete sample recovery proved a problem in the floodplain alluvium. When samples contained clay the recovery was around 75%, but when samples were primarily sand the recovery was as low as 25%.

The Geoprobe® can only penetrate unconsolidated materials. Underlying the alluvium is the Permian Hennessey shale bedrock. Once the Geoprobe® reached the shale, the penetration slowed or stopped completely ensuring complete coverage of the alluvium.

Core Description

Cores were described in the laboratory. They were stored upright to prevent mixing of the sediments. The core liner was split open when the cores were described, but they were kept sealed until then to prevent desiccation. The cores were described using a standard strip-log form. Core was described at a scale of 2.5 cm (1 inch) of strip log to 0.3 meter (1 foot) of core. The core descriptions included details about lamina and bed thicknesses, lithology, sedimentary structures, color, and estimates of texture (grain size, sorting). Color was determined using a visual comparator (Exxon-Mobil). Sediment texture was estimated using a binocular microscope and a grain size/sorting visual comparator. Grain size/sorting estimates were taken about every 0.46 meters (1.5 feet), and each sediment sample averaged about 1 to 2 grams. A range was recorded for the grain size of each sample. This range included the smallest to largest grain viewed in the sample. Then an average grain size was assigned to the sample based on the most frequent grain size seen in the sample.

After the core description was complete for each well, the core was photographed with Kodak 100 film. Each photograph of the core covered about 6.1 meters (20 feet) of the alluvial section, so a set of two photos was required to cover each well. In addition, photographs were taken of key features (texture, structures, bounding surfaces, lithoclasts) within the cores. The negatives from each core were scanned to create digital image files. The images were then inserted to Powerpoint and pieced together.

Texture Analysis of Core Samples

Once the cores were described and photographed, they were broken up into samples for mechanical sieving. About 15 samples were taken from each of the 78 cores, and the average weight of each sample was about 150 grams. Samples were taken whenever there was an abrupt contact or change in grain size within the core. The grain size estimates performed on the cores during the description process helped to identify any key changes in grain size.

The core samples were placed into labeled sample bags. Each sample was sieved through a set of thirty wire mesh sieves using a Ro-Tap machine. The sieves ranged in size from 1 to 230 according to the U. S. Standard Sieve number. This range is equivalent to –4.64 to 4.00 phi

grain size (25.0 to 0.0625 mm). Each core sample was sieved for about 12 minutes. The amount of sediment collected in each mesh was weighed and recorded in grams using a digital scale.

The results from the sieve data were input to an Excel spreadsheet. The spreadsheet was designed to automatically calculate the weight percentages of the individual grain size fractions present in each core sample. These weight percentages were summed to form a cumulative weight percentage curve that was then plotted against phi grain size to form a standard grain size cumulative curve. A cumulative curve was generated for each sample . Each curve was then used to determine a graphic mean and inclusive graphic standard deviation for that sample. The graphic mean is equivalent to a mean grain size and the standard deviation is equivalent to sorting. The equation used to calculate the graphic mean is:

$$Mz = (?_{16} + ?_{50} + ?_{84}) /3 \qquad \text{(eq. 1)}$$

The phi grain size was read from the cumulative curves at the 16%, 50%, and 84% marks. By reading the data from these intervals the central two thirds of the grain size data was encompassed. These three values were then averaged to provide a mean grain size for the sample. The equation used to calculate the standard deviation is:

$$?_I = (?_{84} - ?_{16})/4 + (?_{95} - ?_5)/6.6 \qquad \text{(eq. 2)}$$

For this equation the phi grain size was read at 5%, 16%, 84%, and 95% from each of the curves and input into the equation. The inclusive standard deviation is an average of the standard deviation calculated from $?_{16}$ and $?_{84}$, and the standard deviation calculated from $?_5$ and $?_{95}$. This is the best overall measure of sorting because it includes 90% of the distribution (Folk, 1980). The mean grain size and sorting were then used to calculate the permeability.

The equations used to calculate the graphic mean and inclusive graphic standard deviation followed the recommendations of Folk (1980). These equations were used for this analysis because of their inherent sensitivity to the "tails" of the grain size distribution. This sensitivity is important to determinations of sediment grain sorting, a major control on the porosity and permeability of sands.

Texture-Permeability Equation

The raw data (?, ? , grain size, sorting) from the classic Beard and Weyl (1973) paper was used to generate a permeability equation. These raw data were input to an Excel spreadsheet that was imported to SAS (v.8.01). SAS was used for analyzing the relationships among the variables. A step-wise multivariate statistical technique was used to evaluate the controls on the permeability log units. The results indicate the grain size was the most important to the permeability equation. Grain size phi explained 64% of the total variation, while sorting explained 32%. The r^2 value for the multiple regression was 0.97, significant at the $p < 0.001$ level. This value is so high that one suspects that the Beard and Weyl raw data has been adjusted by some additional factor (Shell Research internal results).

The multivariate equation that was produced to calculate the permeability is:

$$\text{Log(permeability)} = 6.190 - 0.495(S_0) - 0.572\ (?gs) \qquad \text{(eq. 3)}$$

or

$$\text{Permeability} = (10)^{6.19 - 0.495(So) - 0.572(?gs)} \qquad \text{(eq. 4)}$$

where S_0 = sorting and ?gs = phiGS.

Interpretation of Conductivity Logs for Texture and Generation of 3-D Block Diagrams

A database was set up in Rockworks 99 that contained the latitude (X), longitude(Y), and surface elevation (Z) for each of the sample locations. The conductivity log curve files were then associated with their sample locations in the database. Once these curve files were imported into Rockworks with their corresponding X, Y, and Z locations, the software was able to plot the conductivity logs as cross-sections and 3-D block diagrams. Digital strip logs for display were also created for each of the 19 cores based on the log form descriptions.

Geomorphology

The second project objective, concerning geomorphology, was accomplished by completing three tasks:

1) map and analyze surface sediments,
2) evaluate the stability of the landfill clay-vegetation cap, and
3) analyze the horizontal stability of the Canadian River.

Surface Sediment Analysis

A map of surface sediment texture was compiled to better understand spatial patterns of deposition on the floodplain. Approximately 350 samples were extracted from the uppermost 30 cm (1 foot) of the surface using a hand-held auger. The position of each sample was determined using a portable Global Positioning System; samples were acquired with a 37-meter (121 feet) spacing. The texture of each sample was estimated using the "texture-by-feel" method of Northcote (1979). Sediment texture classes were determined using a standard sand-silt-clay ternary diagram. These data were used to derive a polygon map of surface sediment texture using ArcInfo and ArcEdit.

Evaluation of Landfill Cap Stability

The stability of the landfill cap was evaluated to determine its resistance to fluvial erosion during floods. This cap, composed of clay and heavily vegetated, was emplaced in 1985 in an effort to protect the landfill from erosion. The landfill contains two cells, designated east cell and west cell, and measurements were taken on the south slope of each cell, at 15-meter intervals, for a total of 47 sample sites. Measurements were acquired one meter above the base of the landfill, since this would be the area initially affected by either flooding or natural stream migration. The position of each sample was determined using the same portable GPS.

At each sample point, a hand-held penetrometer was used to measure the compressive strength of the cap in units of kg/cm^2. The penetrometer was pressed into the sediment to a designated depth, and the value was read on the scale within the device. Two different sets of measurements were taken with the penetrometer. First, we took a reading on the surface, since this would be the first to be eroded in the case of stream inundation. Then, we took a reading on the sediment pulled out with the auger. There was a very large difference between the two sets of values, mostly due to the presence of an incoherent organic soil layer above the cohesive clay cap. Instead of averaging the two sets of measurements, each was taken independent of the other. This assured that equal weight was given to both sets of values, since the organic upper

layer and the clay lower layer would both be affected, although at different times, during a flood event.

The percent vegetation cover was estimated within a one meter square area around each sample point using visual charts prepared by Hodgson (1974). Vegetation, as used here, is defined as all above-ground living biomass that has a root system and therefore offers stability to the landfill cap, rather than simple ground litter which would wash away immediately upon contact with stream flow.

The final measurement taken was the slope gradient of the landfill at each site. From the top of the landfill, a clinometer was sighted down the face of the landfill to determine the slope angle. The lower the slope angle, the higher the degree of stability of the landfill at that site.

All values were entered into a Microsoft Excel spreadsheet. For each variable (penetrometer reading for the soil and the clay cap, vegetation percentage and slope angle), a mean and a standard deviation were calculated. With this information, a Z score was determined using the following equation:

$$Z = \frac{\text{numerical value} - \text{arithmetic mean}}{\text{standard deviation}} \qquad \text{(eq. 5)}$$

Once this value had been determined, a composite Z score was calculated according to the following formula:

$$Z_{composite} = Z_{soil\ permeability} + Z_{clay\ permeability} + Z_{vegetation} - Z_{slope} \qquad \text{(eq. 6)}$$

In doing this statistical transformation, the values are all normalized and can be compared to one another. Once all z-scores were calculated, a percentile rank was established at the 33% and 67% values. All z-scores below the 33% value were assigned a rank of one, meaning that those areas were the least stable when all variables were taken into account. Z-scores between the 33% and 67% values were assigned a rank of two (moderately stable), and those above the 67% value were assigned a rank of three (most stable). These values were plotted, using ArcInfo and ArcEdit, on the same map as the surface sediments and were color coded according to the designated rankings.

Stream Stability Analysis

The lateral migration of the Canadian River was assessed to determine the likelihood that the landfill could be impacted by channel erosion. This analysis utilized 13 aerial photographs spanning from 1937 to 1997. Curtis and Whitney (2000) had digitized these photos to show the landfill, bankfull stage of the channel, and low-flow active channel. The aerial photos were registered to one another and a grid was created as an overlay, with each grid cell have dimensions of 53 meters by 53 meters. Each aerial photo was inspected in turn to determine whether or not the low-flow active channel occupied each grid cell. The number of times the low-flow channel occupied each cell was tabulated from which the probability of channel occupation for each cell could be calculated. The horizontal and vertical distance from each cell to the low-flow channel was also measured.

Principal Findings and Significance:

Cores from wells 1,3,7, and 46 provide some of the best examples of the sedimentary features noted in the 19-cored wells. The depth units are expressed in English units rather than metric units as the Geoprobe probe rods are manufactured in increments of 4' lengths.

Well #1 Core has a thin, incipient soil (b), mud rip-up clasts (b), and a sharp contact of sands with the underlying mud layer (b). No cross bedding is obvious in the sand beds.

Well #3 Core shows an excellent example of an accumulation of silt and clay that has been carried past the piston by flowing water (due to sudden pressure drop in the core barrel (b). This well also has mud clasts and a solid contact with the underlying Hennessey Fm.

Well #7 Core shows an excellent recovery of gravel near the base of the valley fill and a very sharp contact with the underlying Hennessey red bed (b). Mud in this core is both red and black (organic-rich).

Well #46 Core has some of the best-preserved cross bedding in any of the 19 cored wells. We noted that sedimentary structures were always absent or disturbed below the water table due to rapid movement of water into the well bore during penetration of the probe. The preserved tough cross bedding in this well occurred above the water table (b). Disruption (doming) of layering due to water movement is apparent in images 11b and d. Poorly sorted gravels were recovered near the base of the well (c). Image 11e contains two fining upward cycles, each with gravel at the base.

Criteria for Correlating the Conductivity Logs

The vertical succession of the point bar from the basal contact with the underlying Permian Hennessey Fm. to the present day land surface was vertically subdivided on the basis of conductivity profiles, mud layers, and rapid changes in sediment texture (grain size, sorting). We have no strong independent age-control on the stratigraphy of the point bar. Consequently, the criteria used for correlating the conductivity logs were:

1) similarities in conductivity response patterns,
2) stratigraphic position (superposition), and
3) lithologic similarity.

Our correlation style was strongly tempered by observations about the nature and distribution of the modern Canadian River floodplain sediments.

1) Floodplain: very flat with little relief
2) Sand Bars:
    a) Initially sinuous-crested linguoid-shaped dunes that form during high discharge events dissection of the constructional bar forms by braids of channelized flow that accompany waning flow
    b) incision of the constructional bar forms continues until the occurrence of the next high discharge event
3) Mud Layers

a) Occur adjacent to main channels; are flat-topped, may onlap an erosional surface, are discontinuous
b) mud layers develop as silt and clay settles from suspension each time high water (which has a high suspended load in the Canadian River) inundates the topographic lows on the floodplain
c) the topographic lows are the erosional features mentioned above and are produced subsequent to a high-discharge event

In this sense, the internal morphology of a bar-form in the Canadian River is constructional while erosional processes have shaped the external morphology. Subsurface evidence confirms these observations with respect to bar form shape and relationship to mud layers. The contacts of mud layers with underlying bar sands were observed in core to sometimes onlap erosional surfaces and vice versa. In addition, mud clasts are found at the base of some of the sandbars. The mud clasts were derived from the mud layers as the river reasserts itself and erodes the surface sediments during a high discharge event.

Conductivity Cross Sections

Cross-sections of the conductivity logs were correlated across the study area. Eleven cross-sections were created. Six of the cross-sections run perpendicular to the point bar and five run parallel to the point bar. Two cross-sections are included here: Cross-section D-D' runs perpendicular to the point bar, and a portion of cross-section I-I' runs parallel to the point bar.

The cross-sections indicate that the gross stratigraphy of the floodplain is essentially horizontal (layer-cake) and similar to flat floodplain topography seen today. The floodplain alluvium was broken up into 5 intervals that are labeled as Unit 100 through Unit 500. These units are identified on each of the cross-sections.

Unit 100: Basal layer of the alluvium. It ranges in thickness from 1.8 to 2.4 meters (6 to 8 feet) from the base of the alluvium. This unit is characterized by coarse-grained sediments and gravels.

Unit 200: Sand overlying the basal layer. It is about 3 m (10 feet) thick.

Unit 300: Unit overlying the 200 unit. It ranges in thickness from 4.5 to 6 m (15 to 20 feet). This layer contains extensive mud layers and lenses.

Unit 400: Sand unit overlying the 300 unit. It is about 2.4 to 2.7 m thick (8 to 9 feet).

Unit 500: Unit extending from the surface down to about 1 m (3 feet). This unit is composed of very fine-grained sands.

These intervals each have distinct texture (grain size/sorting) and are bounded by mud layers. Mud layers were drawn on the cross-sections to illustrate the number and thickness of the muds in the floodplain alluvium. The cross-sections indicate that the number and thickness of muds increases toward the slough. The lateral extent of the mud layers throughout the alluvium is as follows:

1) Mud layers perpendicular to the bar complex range in length from <37 meters (<120 feet) to about 148 meters (485 feet)
2) Mud layers parallel to the bar complex range in length from <37 meters (<120 feet) to about 222 meters (728 feet)

Vertical Profiles and Interval Units for Correlation

A Type Conductivity Log shows the standard vertical succession of sand and mud encountered in the 19 cores taken from the point bar. The lower 6-8' of the fill yields a characteristic 'choppy' conductivity response that is related to the basal layer (our *100 Interval*) deposited on top of the underlying Permian Hennessey Formation. The frequency distributions of grain size and sorting for the basal layer are negatively skewed and bimodal. One mode is medium grained (0.25-0.5mm) and moderately sorted. The other mode is very coarse grained (0.5-1mm) and poor- to very poorly sorted. Some wells contain granule- (2-4mm) and pebble-size materials (>4mm).

At this point, we are unable to see any geographic significance to the bimodality. The bimodality may reflect inadequate sample size for such a heterogeneous population (n=55). The texture (grain size / sorting) of the basal layer is distinctly different from the texture of all the overlying layers on the basis of a Satterthwaite[?] t-test ($p < 0.0001$) performed in SAS, v. 8.01, 1999-2000 (Tables 2, 3). The null hypothesis (H_o) for this test assumes that the means for the two populations are equal (or not different). In this exercise, we assumed a real difference to exist between populations means if $p < 0.1$.

A well developed but discontinuous mud layer (1-3' thick) is commonly present above the basal gravel. The overlying sand layer (*Interval 200*) is about 3 meters (10 feet) thick. This interval is fine to medium grained and moderately to moderately-well sorted. A few of the wells in this interval contain coarse grained, poorly sorted sand.

Another discontinuous interval of mud lenses (1-3' in thickness) lies above *Interval 200*. The *300 Interval* is fine to medium grained and moderately to moderately-well sorted. This interval is the thickest (about 15-20') and most heterogeneous of the layers with respect to the occurrence of mud layers and lenses. A t-test suggests that *the 300 Interval* mean grain sorting is significantly different from the underlying *200 Interval* ($p < 0.0001$). The grain sizes between the two layers are slightly different ($p < 0.08$) (Tables 2, 3). Another 1-3' thick mud lenses occurs throughout the point bar at a depth interval between 5 and 10'.

The *400 Interval* is 2.4-2.7 meters (8-9 feet) thick and contains fine-grained, moderately-well to well sorted sand. T-tests again indicate that the 400 Interval sand is finer grained ($p < 0.04$) and better sorted ($p < 0.01$) than the underlying *300 Interval*.

The *500 Interval* extends from the surface down to about 1 meter (3 feet). This unit is fine to very-fine grained and moderately-well to well sorted. The *500 Interval* is significantly different from the underlying *400 Interval* with respect to grain size ($p < 0.0001$). Sorting does not vary between the *500 and 400 Intervals* ($p < 0.85$). The textural character of this upper layer is shaped by both soil forming processes and aeolian sedimentation.

Calculated Permeabilities Relative to Stratigraphic Intervals

A SAS (v. 8.01) step-wise multivariate analysis of the grain size, sorting, and permeability data taken from the experiments of Beard and Weyl was performed. The intent of this analysis was to estimate the relative importance of grain size and sorting in controlling the

[?] Satterthwaite assumes unequal variances

permeability of the grain packs used in their experiments. This analysis indicates that phi grain size explains 60% of the variation in permeability. This is followed in importance by grain sorting, which accounted for another 37% (60 + 37 = 97% total variation in permeability accounted for by these two variables). This analysis and inspection of the permeability equation (eq.4) suggests that point bar permeability will increase strongly with increasing grain size and vice versa. Likewise, better-sorted sands will have higher permeability, but this tendency can be offset quickly if the grain size grows small, resulting in lower permeability.

Accordingly, the vertical permeability profile for all the sieve data[?] suggests that permeability varies more strongly with grain size than with sorting. Consequently, the permeability profile appears more similar in shape to the grain size profile than to the sorting profile. The basal *100 Interval* (in red) exhibits the highest calculated permeabilities in the profile due to a population of large grains. This high permeability population has not been offset by the potential reduction in permeability due to poor sorting. Clearly, calculated permeabilities would be much higher if the coarsest grained Norman Landfill point bar sediments were better sorted. Likewise, the rapid fall in permeability in the *500 Interval* at the surface is due to a strong grain size shift to very fine-grained sand in these moderately-well sorted sands.

T-tests were performed on the permeability populations to determine if real permeability differences exist between the layers of the point bar. The basal *100 Interval* permeability is significantly different from the overlying *200 Interval* ($p < 0.0001$). The *200 and 300 Interval* permeabilities are not significantly different from one another ($p < 0.47$). Likewise, the *300 and 400 Intervals* are essentially the same with respect to permeability ($p < 0.19$). The mean permeability of the *500 Interval* population is significantly different from the underlying *400 Interval* ($p < 0.002$). These tests are summarized in Table 4.

Permeability and Fining Upward Profile of Fluvial Sediments

Vertical profiles of the sieve data indicate that the 'classic fining-upward' profile for fluvial systems is punctuated at both the channel base and at the top by rapid changes in grain size and / or sorting (at least for the Canadian River). The *100 Interval* displays a very rapid yet progressive grain size decrease and improvement in size sorting from the channel base to about 8' up from the base. Likewise, the grain size of the upper few feet (*500 Interval)* of the point bar is much finer grained. As mentioned above, this rapid shift to finer grain size is due primarily to aeolian reworking of the floodplain sediments.

Excluding these deepest and shallowest intervals, the grain-size sorting improves progressively from 30' to a depth of about 3'. Grain size does not change very much through the base of the *200 Interval* to the top of the *400 Interval* . Visual inspection of the grain size trends in the thick *300 Interval* shows no vertical variation in grain size. The statistically significant differences in grain size noted earlier for the *200 to 400 Intervals* (upward fining) appears to not be translated to an upward decrease in permeability. This finding appears compatible with the following observations: (1) the vertical grain size differences are quite subtle and (2) there is a concomitant improvement (statistically significant) in grain sorting. The improved grain sorting has resulted in higher porosity that compensates for the progressively decreasing grain size upward.

The work of Christensen et al. (1998) used slug tests and calculations of hydraulic conductivity to conclude that the highest permeability in the alluvium adjacent to the NLF is

[?] calculated from an equation generated from data published by Beard and Weyl, 1973

located at the base of the sediment package. The vertical permeability profile in for the NLF is similar in appearance to the data of Christensen et al. (1998).

Conversion of the NLF permeabilities calculated from sieve data to hydraulic conductivity values yields a profile that is also similar in appearance to the Christensen et al (1998) data. The present study concurs with the findings of the Christensen et al. (1998) and finds significant evidence for a preferred permeability pathway at the base of the alluvial fill. However, the sand intervals above the base (with exception of the 500 Interval near the surface) all have comparable permeability.

The calculated hydraulic conductivity resulted in a range from 1.4E-04 m/s to 9.22E-04 m/s. The higher hydraulic conductivity was seen in the basal segment of the alluvium. It was estimated that the plume is moving at rate of at least 48 meters per year in the basal unit. This estimate was calculated using a gradient of .0006 that is characteristic between the floodplain and the slough. However, the gradient becomes steeper as you approach the slough so the rate of plume movement may increase. This rate of movement also decreases shallower in the section as hydraulic conductivity of the sediments declines.

Texture and permeability profiles for Wells #1 and 15 were examined.. In some of the wells, the correspondence between grain sizes, sorting, and conductivity is quite striking. The correspondence suggests that lower conductivity sand intervals are finer grained and better sorted than higher conductivity sand intervals. We do not understand this relationship. The data would suggest that deeper, coarser grained and more poorly sorted sand intervals contain more disseminated silt and clay than the shallow sand intervals. We see no evidence for this in our cores.

Block Diagrams

Block diagrams were created of the floodplain alluvium. They provide a 3-D perspective of the geometry and thickness of the 5 distinct sand intervals in the point bar. There are 6 block diagrams. Three view the study area from the southwest corner, and three view it from the southeast corner. Both the southwest and southeast view are illustrated with 25%, 50%, and 75% of the model cutaway. These diagrams provide a 3-D view of the gross stratigraphy of the floodplain. As determined by the cross-sections it is essentially horizontal (layer-cake) and similar to the flat floodplain topography seen today.

Block diagrams of the conductivity data were also created. These diagrams provide visuals of changes in conductivity throughout the floodplain. Two diagrams were made of the entire study site. One is viewing the site from the southeast corner and the other is viewing the site from the southwest corner. Higher conductivity values near the slough are apparent between 1055 and 1075 feet. These higher conductivity zones are near Wells #23 and #28, which are between the slough and the landfill. Thick, dense clay layers were found in these cores about 1070 feet, which is 15 feet below the surface.

Conductivity slices were also created for each of the five sediment intervals. The slices provide visualization of conductivity changes with depth. By comparing each of the slices it is seen that there is not much differentiation in conductivity in the west side of the study area. The highest conductivity zones are limited to the area adjacent to the landfill. In the east side of the study area there is very high conductivity seen in the base of the 200 Unit. This high conductivity zone is associated with the thick, dense clay as seen in cores 23 and 28. The conductivity in this zone remains high near the landfill and decreases as you move further west.

Conductivity near the landfill is higher than expected for clay rich sediment, and may suggest interaction of the clay with the leachate.

The high conductivity zone seen adjacent to the landfill appears to extend vertically through units 400, 300, 200 and 100. The conductivity values then begin to decline as you move away from the landfill towards the floodplain. These elevated conductivity values could be due to the increase in number of muds in the east side of the study site. However in our observations we did not see a significant enough increase in muds as to result in a distinction between east and west sides of the study area. Therefore, it could be possible that the leachate contamination is reflected in the higher conductivity areas. However, there is not enough information to distinguish between what may be the plume or may be clays.

Surface Sediment Analysis

The map created with the surface sediment data shows some patterns distinctive of meandering to braided stream systems. There are obvious ripple and dune complexes with interdune areas composed of much finer material, which is indicative of gradual channel migration. Topographically low areas contain a substantially larger proportion of fine-size sediment than the surrounding higher areas. In addition, the sand observed in this particular environment behaves as quicksand when located close to the water table.

Grain size on the surface of the floodplain is rarely larger than medium to coarse sand, and the dune areas exhibit distinct longitudinal patterns running parallel to the channel. These units are similar to the longitudinal bars found in braided streams, although the grain size is smaller than usually found in common braided systems. The reason for this is most likely its distance from source, which may be found in southeastern Colorado.

In most natural river systems like the Canadian River, this pattern of dune highs with muddy interdune lows can be followed down the floodplain. In our study area, it may be noticed that there is an obvious discontinuity of sediment patterns from the northwest portion of the map area toward the southeast. An asphalt company extracts sand from the floodplain and active channel. One entire section of the frontal dunes that lie immediately adjacent to the river has been removed, as well as most of the inland dunes toward the asphalt plant. This activity has disrupted the expected patterns of sediment texture on the floodplain. Sediment in this area is so fine that the threshold for erosion and entrainment is very low. In addition, the mean elevation of the southeast portion of the floodplain is noticeably lower than the northwest. Any inundation of the stream, either by natural migration or by flood activity, will pass over the southeast portion of the floodplain without barrier until it reaches the landfill.

Landfill Stability Analysis

Patterns created by the landfill stability data yielded some interesting yet relatively inconclusive results. Results attained from this study do not necessarily show that there is a preferred region of either instability or stability within the landfill itself. The clay cap is generally homogeneous and becomes very hard upon exposure to the sun. In the event of a flood or natural stream migration to the base of the landfill, though, the clay would again become saturated and would lose any inherent stability it would otherwise have if it were "baked." The clay that composes the landfill cap is tacky and highly cohesive. From external observation only, it also seems to increase in thickness toward the bottom of the landfill, simply from downslope sediment movement. Portions of the landfill that protrude furthest into the path of floodwaters are no less stable than other portions of the landfill. A 1986 peak flow of 2180 cms, a 15-year event,

removed rip-rap protection for the landfill, penetrated the clay cap, and eroded 5013 m^3 of landfill contents.

Stream Stability Analysis

The probability map of channel location reveals several specific areas of the floodplain that are particularly prone to channel inundation. It is interesting to notice that the area of the floodplain nearest the landfill has relatively high probability values. An overflow channel exists (the "slough") that runs parallel to the base of the landfill. Whenever the level of the river reaches flood stage, water travels through the slough and erodes material from the base of the landfill.

The probability, horizontal distance to the channel and vertical distance to the channel were log-normally distributed. Multiple regression analysis was performed to determine the controls on probability. The r^2 value for the multiple regression was 0.30, significant at the $p < 0.001$ level.

$$\text{Log}(P) = 2.44 - (0.605)(\text{LogLD}) - (0.251)(\text{LogUD}) \quad \text{(eq. 7)}$$

or

$$P = 275(\text{LD})^{-0.605}(\text{UD})^{-0.251} \quad \text{(eq. 8)}$$

where P is the probability of stream presence, LD is the lateral distance to the low-flow channel (in meters) and UD is the upstream/downstream distance to the river channel (in meters).

CONCLUSIONS

Principle findings of the study are as follows:

1) On the basis of conductivity patterns, sediment texture, and vertical succession, five distinct layers are seen throughout the floodplain area. Of these, the basal layer will be the most significant in the transport of the plume. Earlier studies based on specific conductance of the groundwater have determined that the plume is already in this layer.
2) The flow pathways are bounded by mud layers that are discontinuous. These mud layers are found in similar stratigraphic positions and were likely formed during periods of time when the surface was exposed. Some layers do appear to be more extensive throughout the area. The dimensions of these larger mud layers are:
    a) Mud layers perpendicular to the bar complex range in length from <37 meters (<120 feet) to about 148 meters (485 feet)
    b) Mud layers parallel to the bar complex range in length from <37 meters (<120 feet) to about 222 meters (728 feet)
3) The number and thickness of mud layers increases toward the slough (adjacent to the landfill.
4) The maximum permeability pathway (as defined by grain size / sorting) is located in the basal segment of the valley fill. This interval encompasses the lower 1.8 to 2.4 meters (6 to 8 feet) of the alluvium and has an average permeability of 105 Darcies.
    a) The sediment overlying the basal unit has a permeability of 38 Darcies. This encompasses units 200, 300, and 400 for a total thickness of about 8.6 meters (28 feet).
    b) The sediments in the upper 0.6 meters (2 feet) of the alluvium have a permeability of 16 Darcies. These sediments are mainly aeolian.
5) Block models of the different sand units provide a 3-D view of the geometry and thickness of the 5 distinct sand intervals in the point bar.

6) Conversion of permeability data to hydraulic conductivity resulted in a range from 1.4E-04 m/s to 9.22E-04 m/s. The higher hydraulic conductivity was seen in the basal segment of the alluvium. This data compared very favorably to hydraulic conductivity measurements taken by Scholl and Christenson (1998).
7) It was estimated that the plume is moving at a rate of at least 48 meters per year in the basal unit. This estimate was calculated using a gradient of .0006 that is characteristic between the floodplain and the slough. However, the gradient becomes steeper as you approach the slough so the rate of plume movement may increase. This rate of movement also decreases shallower in the section as hydraulic conductivity of the sediments declines. Our estimate of the plume movement is higher than previously reported.
8) Block models were also created of the conductivity data. These models show higher conductivities near the landfill and slough. This supports the findings that the number and thickness of muds increases as the slough is approached. A thick, dense clay layer is located about 4 meters below the surface between the landfill and the slough (well 23 and 28). This clay is highly conductive as compared with the rest of the landfill alluvium and does not appear in cores away from the slough.
9) On balance, much higher conductivities are found in the areas near the slough and landfill. This is in part due to the number of clays in the area. Moreover, the base conductivity level for clean sands in this area is much higher than seen in most of the floodplain sands. Therefore, it is possible these higher conductivities are an indication of direct detection of the leachate plume with the Geoprobe conductivity tool.
10) The pebbles and gravels in the high permeability zones are not derived from the bedrock in the vicinity of Norman, Oklahoma.
11) The pattern of sediment deposition that one expects on a floodplain has been found only on the upstream end of the floodplain adjacent to the landfill. Asphalt plant mining operations have disrupted the pattern elsewhere. The majority of the floodplain is mantled with aeolian sediment, reworked from fluvial deposits during the low-flow season.
12) Lateral migration of the thalweg Canadian River is frequent, as expected for a low-gradient, sand-bed river. The thalweg has been positioned near the base of the landfill approximately 15 percent of the years between 1937-1997. The position of the thalweg indicates where maximum stream power is likely to be directed during flood events. The cross-section analyses completed in this study indicate that vertical scour of floodplain alluvium during flood events may reach six meters (20 feet). Any portion of the plume within six meters of the surface can be expected to enter the Canadian River faster through erosion than it would by movement through the alluvium.
13) The landfill cap does exhibit a range in stability but no spatial pattern to the stability is evident. The base of the landfill remains subject to direct attack by flood flows, including rather peak flows of relatively high frequency and low magnitude. Additional protection of the base of the landfills on the south side may be warranted to prevent direct erosion of the landfill contents as had occurred in the past.

REFERENCES

Beard, D. C. and P. K. Weyl, 1973, Influence of texture on porosity and Permeability of Unconsolidated Sand: AAPG Bulletin, v. 57, no. 2, p. 349-369.

Boggs, Sam Jr., 1995, Principles of Sedimentology and Stratigraphy: Prentice Hall, New Jersey, p. 520.

Curtis, Jennifer and Whitney, John W. 2000. Geomorphology and flood hazards at a toxic landfill on the Canadian River floodplain, central Oklahoma. Preliminary draft of a USGS report.

Folk, Robert L., 1980, Petrology of Sedimentary Rocks (Second Edition): Hemphill Publishing Company, Austin, Texas, p. 42-43, 184.

Geoprobe Systems. www.geoprobesystems.com

Hodgson, J.M. (ed.). 1974. Soil Survey Field Handbook. Soil Survey Technical Monograph no. 5, Harpenden, Rathamsted Experiment Station.

Northcote, K.H. 1979. A Factual Key for the Recognition of Australian Soils. Adelaide, South Australia, Rellim Technical Publications.

Scholl, Martha A. and Scott Christenson, 1998, Spatial Variation in Hydraulic Conductivity Determined by Slug Tests in the Canadian River Alluvium Near the Norman Landfill, Norman, Oklahoma, USGS, Water Resources Investigations Report 97-4292, p. 1-28.

Information Transfer Program

Activities for the efficient transfer and retrieval of information are an important part of the Environmental Institute/OWRRI program mandate. The Institute maintains a web site on the Internet at URL http://environ.okstate.edu/ that provides information on the OWRRI and supported research. The site provides links to information on publications of the institute, grant opportunities and deadlines, and any upcoming events. A listing of technical reports and other publications generated by OWRRI and other Environmental Institute sponsored research is updated regularly and is accessible on the Institute homepage. The publication of the bi-monthly newsletter of the Institute has continued. Prism, is a valuable source of information on research activities sponsored by the Institute and research opportunities in water resources and environmental research. It also announces the availability of new publications from the Institute and reports and publications received by the Institute and forwarded to the library. Prism may be accessed at the Institute web site. Also available through the web site is a listing of Technical Reports and General Publications generated by OWRRI sponsored researchers and the Environmental Institute. Abstracts of each of the publications are available.

USGS Summer Intern Program

Student Support

Student Support					
Category	**Section 104 Base Grant**	**Section 104 RCGP Award**	**NIWR-USGS Internship**	**Supplemental Awards**	**Total**
Undergraduate	3	0	0	0	3
Masters	4	1	0	0	5
Ph.D.	0	2	0	0	2
Post-Doc.	0	0	0	0	0
Total	7	3	0	0	10

Notable Awards and Achievements

None

Publications from Prior Projects

None